ISTANBUL TECHNICAL UNIVERSITY ★ GRADUATE SCHOOL OF SCIENCE ENGINEERING AND TECHNOLOGY

CFD APPLICATIONS for SEAKEEPING CALCULATIONS of FLOATING BODIES

M.Sc. THESIS

Burak Tunç ÇEKİRDEKÇİ

508111114

Department of Shipbuilding and Ocean Engineering

Shipbuilding and Ocean Engineering Master Program

Thesis Advisor: Prof. Dr. Kadir SARIÖZ

JANUARY 2015

<u>İSTANBUL TEKNİK ÜNİVERSİTESİ ★ FEN BİLİMLERİ ENSTİTÜSÜ</u>

YÜZER CİSİMLERİN DENİZCİLİK HESAPLARI İÇİN CFD UYGULAMALARI

YÜKSEK LİSANS TEZİ

Burak Tunç ÇEKİRDEKÇİ

508111114

Gemi ve Deniz Teknolojisi Mühendisliği Ana Bilim Dalı

Gemi ve Deniz Teknolojisi Mühendisliği Yüksek Lisans Programı

Tez Danışmanı: Prof. Dr. Kadir SARIÖZ

OCAK 2015

Burak Tunç ÇEKİRDEKÇİ, **a M.Sc.** student of ITU **Graduate School of Science Engineering and Technology** student ID 508111114, successfully defended the **thesis** entitled "**CFD APPLICATIONS for SEAKEEPING CALCULATIONS of FLOATING BODIES**", which he prepared after fulfilling the requirements specified in the associated legislations, before the jury whose signatures are below.

Thesis Advisor : **Prof. Dr. Kadir SARIÖZ** ....

İstanbul Technical University

Jury Members : **Prof. Dr. Kadir SARIÖZ** ....

İstanbul Technical University

Prof. Dr. Abid KÜKNER ....

İstanbul Technical University

Prof. Dr. Ahmet Dursun ALKAN ....

Yıldız Technical University

Date of Submission : 12 December 2014

Date of Defense : 22 January 2015

FOREWORD

I would like to express my gratitude to my esteemed professor Prof. Dr. Kadir SARIÖZ for his interest and sympathy, supporting me and sharing his knowledge and experience in every step of my thesis study.
I would like to thank to Asst. Prof. Yalçın ÜNSAN for his invaluable guidance and personal encouragement.

I would also thank to my friend Burak CAN for supporting me during my post graduate period and professional & personal life.

I appreciate the patience and understandings of the staff of FIGES especially Tayfun GÜLEM during my post graduate period.

I am grateful to my family for their understanding and support during my whole life.

Last, but not least, I would like to thank my partner ELİF PINAR. Without her support, understanding and encouragement, this study would never have been completed.

January 2015

Burak Tunç ÇEKİRDEKÇİ
Shipbuilding and Ocean Engineer

TABLE OF CONTENTS

Pages

ABBREVIATIONS

3D	:	Three dimensional
A, A_W	:	Waterline area
A_y	:	First moment of inertia of waterline area
A_{xy}, A_{xx}	:	Second moment of inertia of waterline area
A_{jk}	:	Added mass matrix
a_{33}	:	Sectional added mass
b_{33}	:	Sectional radiation damping
B	:	Breadth of ship
B_{jk}	:	Radiation damping matrix
C_{jk}	:	Hydrostatic restoring matrix
C_B	:	Block coefficient
C_M	:	Midship coefficient
C_P	:	Prismatic coefficient
C_{WP}	:	Waterplane coefficient
D	:	Depth of ship
f_j	:	Direction-cosines
Fn	:	Froude number
F_{Ij}	:	j^{th} Froude-Krylov force
F_{dj}	:	j^{th} diffraction force
F_{rjk}	:	j^{th} radiation force due to unit amplitude rigid motion of k^{th}
g	:	Gravitational acceleration
k	:	Wave number
M_{jk}	:	Generalized mass matrix
$\vec{r}$	:	Position vector
RAO	:	Response Amplitude Operator

$\mathbf{k_{XX}}$	:	Radius of gyration around X axis
$\mathbf{k_{YY}}$	:	Radius of gyration around Y axis
$\mathbf{k_{ZZ}}$	:	Radius of gyration around Z axis
L	:	Length of floating body
$\mathbf{L_{BP}}$	:	Length between perpendiculars
$\mathbf{L_{WL}}$	:	Length at the waterline
LCF	:	Longitudinal center of flotation
LCB	:	Longitudinal center of buoyancy
$\mathbf{S_0}$	:	Wetted surface of structure
$\mathbf{u_1}$	:	Surge motion
$\mathbf{u_2}$	:	Sway motion
$\mathbf{u_3}$	:	Heave motion
U	:	Forward speed
T	:	Draft of ship
$\mathbf{u_x}$	:	Velocity of the fluid in x direction
$\mathbf{u_y}$	:	Velocity of the fluid in y direction
$\mathbf{u_z}$	:	Velocity of the fluid in z direction
V	:	Volumetric displacement of structure
$\mathbf{v_j}$	:	The velocity of oscillation body
$\mathbf{v_n}$	:	The velocity of a water particle
z	:	Depth of sea water
$\mathbf{z_b}$	:	Vertical position of center of buoyancy
$\mathbf{z_G}$	:	Vertical position of center of gravity
∇	:	Nabla operator
λ	:	Wave length
ρ	:	Density of sea water
η	:	Displacement of motion
$\dot{\eta}$	:	Velocity of motion
$\ddot{\eta}$	:	Acceleration of motion
ϕ	:	Velocity potential function

ω_n	:	Natural frequency for the n^{th} motion
ω	:	Wave frequency
ω_e	:	Encounter frequency
μ	:	Wave heading
ζ_a	:	Wave amplitude
θ_4, θ	:	Roll motion
θ_5, φ	:	Pitch motion
θ_6, ψ	:	Yaw motion
θ_a	:	Rotation in radian
ε	:	Phase angle

LIST OF TABLES

LIST OF FIGURES

Page

CFD APPLICATIONS for

SEAKEEPING CALCULATIONS of FLOATING BODIES

SUMMARY

Seakeeping calculations are very complex due to dynamics of fluid and the characteristics of the motions. Two fundamental problems are solved to calculate the seakeeping performance of a vessel. The first of these is the hydrodynamics problem which is about wave exciting force and the other is dynamic problem which is relevant to the motions due to wave exciting forces. Also to obtain the motions in waves, added mass and damping forces of the vessel have to be calculated.

Strip theory is one of the most popular methods to predict the hydrodynamic forces and motions. Very accurate results are obtained for conventional ships by the strip theory and a number of software based on this theory are widely used by the shipbuilding and offshore engineering industry around the world. However, as a consequence of development of new ship forms and unconventional offshore structures 3D panel methods have been developed for the cases where the strip theory is not applicable.

Rapid development of CFD based hydrodynamic analysis software in recent years has resulted in the application of CFD based computational methodologies for seakeeping problems. The main goal of this study is to show the feasibility of CFD based methods for predicting seakeeping performance characteristics in a mathematically described seaway. For this purpose a typical CFD software (AQWA) based on 3D panel method was selected.

Four different case studies are performed to validate the linear seakeeping theory. First, the experimental results of added mass and damping coefficients of rectangular, triangular and cylindrical shaped floating bodies are compared with AQWA results. Second, the results of the calculations by strip theory of a rectangular barge are compared with those obtained by AQWA. The third comparative study is relevant with Series 60 formed ships. In the last study, the results of experiment, which is predicted the motions and accelerations of DTMB 5415 model based on the DDG51 type US Navy Combatant form, are compared with AQWA results. Comments about all studies are presented in CONCLUSION & FUTURE WORKS section.

YÜZER CİSİMLERİN DENİZCİLİK HESAPLARI İÇİN

CFD UYGULAMALARI

ÖZET

Denizcilik hesapları, akışkan dinamiğinden ve hareketlerin karakteristiklerinden dolayı oldukça karmaşıktır. Yüzer bir yapının denizcilik performansını hesaplayabilmek için iki ana problemin çözülmesi gerekmektedir. Bunlardan ilki, dalga kaynaklı zorlayıcı kuvvetlerle ilgili olan hidrodinamik problemdir. Diğer ana problem ise bu kuvvetlerden kaynaklanan yapı hareketlerinin incelendiği dinamik problemdir. Yüzer bir yapının dalgalar içerisindeki hareketlerinin belirlenmesinde eksu kütlesi ve sönüm kuvvetlerinin de ayrıca hesaplanması gerekmektedir.

Dilim teorisi, hidrodinamik kuvvet ve momentlerin belirlenmesinde oldukça sık kullanılan bir yöntemdir. Konvansiyonel gemilerin denizcilik hesaplarında, dilim teorisi oldukça başarılı sonuçlar vermektedir. Bununla birlikte dilim teorisi temelinde hazırlanmış olan birçok yazılım, küresel gemi inşa ve açık deniz yapıları sektöründe sıkça kullanılmaktadır. Dilim teorisinin uygulanabilir olmadığı, geliştirilen yeni gemi formları ve konvansiyonel olmayan açık deniz yapılarının tasarımıyla birlikte üç boyutlu panel yöntemi geliştirilmiştir.

Son yıllarda, CFD tabanlı hidrodinamik analiz yazılımlarının hızlı gelişimiyle birlikte, denizcilik problemleri için CFD tabanlı hesaplama yöntemlerine ait uygulamaların sayısı da artış göstermektedir.

Bu çalışmanın temel amacı, denizcilik performans özelliklerinin belirlenmesinde, deniz koşullarının matematiksel olarak tanımlandığı CFD tabanlı yöntemlerin uygulanabilirliğini göstermektir. Bu amaçla üç boyutlu panel yöntemi temelinde geliştirilmiş olan bir CFD yazılımı (AQWA) seçilmiştir.

Lineer denizcilik çalışmalarının doğrulanması adına dört farklı çalışma yapılmıştır. Bunlardan ilki, kare, üçgen ve silindirik kesitli yüzer cisimlerin eksu kütlesi ve sönüm katsayılarına ait deneysel sonuçlar, AQWA sonuçlarıyla karşılaştırılmıştır. İkinci çalışmada, kare kesitli bir dubanın dilim teorisiyle yapılan hesaplamalarına ait sonuçlar, AQWA ile yapılan analiz sonuçlarıyla karşılaştırılmıştır. Üçüncü karşılaştırmalı çalışmada ise Seri 60 formlu bir gemi incelenmiştir. Son çalışma olarak da temel tasarımı, Amerikan Deniz Kuvvetleri’ne ait DDG51 tip muharip sınıf gemi formuna dayanan DTMB 5415 model bir gemiye ait deneysel hareket ve ivme sonuçları AQWA sonuçlarıyla karşılaştırılmıştır. Yapılan çalışmalara ait yorumlar CONCLUSION & FUTURE WORKS bölümünde sunulmaktadır.

1. INTRODUCTION

The basic problem about the floating bodies in waves, which move with or without forward speed, is the dynamic balance of the forces and moments caused by the waves. Since the structure and vibration problems are not considered in seakeeping calculations, rigid body assumption can be made.

The forces generated on the floating body are caused by the gravity and fluid pressure. By neglecting the viscous effects, the motion of the fluid can be assumed irrotational and the problem can be solved with potential theory. In potential flow, the fluid pressure is obtained from Bernoulli Equation via velocity potential and its derivatives. If a ship is in dynamic equilibrium condition, fluid-induced external forces are in equilibrium with the gravitational and inertial forces.

Even it is assumed that the fluid is homogeneous, incompressible and inviscid, the ship motion is a difficult problem to solve. Therefore, the problem is simplified with some linearization. As a result of the linearization, the linear superposition of hydrodynamic problems is allowed by using perturbation analysis. Superposition principle plays a major role in efforts for the solutions. For example, the responses of the ships in irregular waves are considered as the sum of responses of regular waves in all frequencies. Ship motion problem is greatly simplified via linear superposition of motion in regular sinusoidal waves. The problem is merely the solution of the rigid body’s motion equation in a single regular wave.

In calculations performed according to the linear seakeeping theory, accurate results can be obtained for conventional ships. However non-linear effects become important for high-velocity, non-conventional ships and designs like offshore structures or seakeeping calculations in extreme sea conditions.

This thesis focuses on the linear theory. First, background of the linear potential theory is presented. After defining the fluid mathematically, the part, in which the loads caused by fluid and floating body’s dynamics are described, and the kinematic part, in which the load-induced responses of the body are studied, are presented. As shown in Figure 1-1, the fluid-induced forces are analyzed under two main headings. The first heading is the wave-induced hydrodynamic loads. The second heading is hydrostatic restoring force, which is independent in wave frequency.

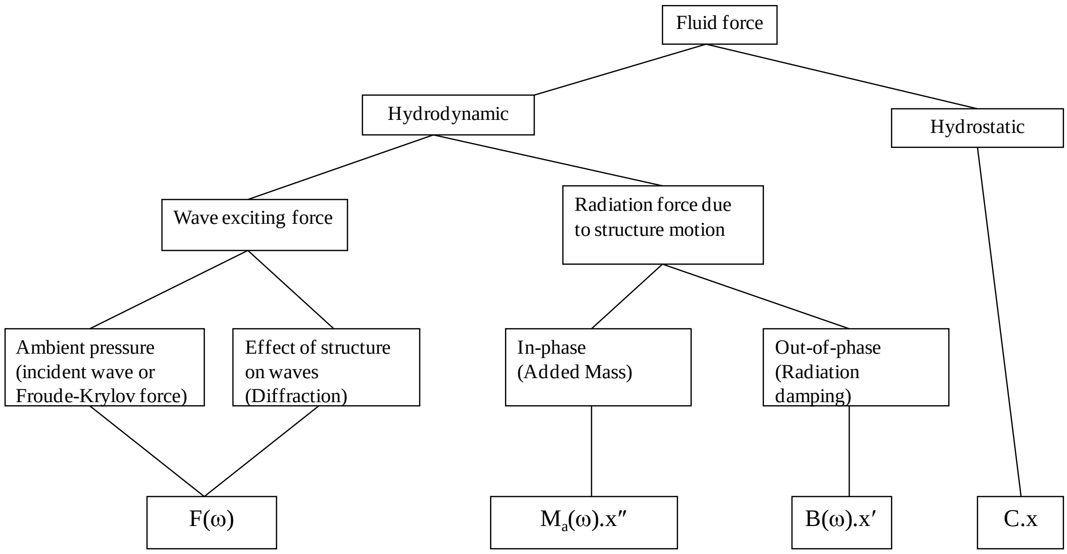

Figure 1-1 : Fluid forces on a floating body (ANSYS, 2014)

Hydrodynamic forces are also divided into two sub-headings in itself. The first force is the wave exciting force arising from the interaction between incident waves and floating body. The other force is the force of radiated waves resulting from the movement of the body in waves. Radiation force is used for calculations of added mass and damping, which are the hydrodynamic characteristics of the floating structure.

Four different studies are implemented by using the obtained theoretical knowledge in practical applications and ANSYS-AQWA software, which is developed on the basis of three dimensional panel method (ANSYS, 2013). First, experimental measurements for two dimensional hydrodynamic coefficients of floating bodies having rectangular, triangular and cylindrical cross sections are compared with the results of AQWA analysis. Next, the seakeeping analysis of a barge having regular rectangular cross section is performed by using strip theory and AQWA. Then the results are compared.

In the latter study, the experimental results of heave and pitch motions of a Series 60 formed ship are compared with the results of AQWA analysis.

Finally, the experimental results for the heave and pitch motions and vertical accelerations of a DTMB 5145 model representing the DDG51 type US Navy Combatant at speeds corresponding to Fn=0 and Fn=0.41, are compared with AQWA results.

2. NUMERICAL METHODS for SEAKEEPING

The calculation of motions of the floating structures in seaway is considerably complex. The sources of this complexity are dynamics of fluid and the characteristics of the motions. The main objective is to provide guidance for the design of floating structures by modeling this chaotic environment mathematically and by achieving realistic results via analysis.

Seakeeping calculations go through the solution of two fundamental problems. The first of these is the hydrodynamics problem which involves the calculation of the wave induced forces arising on the floating bodies. The other main problem is the dynamic problem which involves the solution of the motions which the floating body will show as reaction under the calculated forces. (Okan, 2007)

The solution of the hydrodynamic part is the fluid induced loads which originate from two fundamental problems: Diffraction and Radiation. The diffraction problem causes wave exciting forces on the structure with two components:

- Froude-Krylov force
- Diffraction force

The Froude-Krylov force is generated on the structure by the incident waves regardless of the structure geometry. This component is calculated based on the assumption of that the incident wave has non-distortional form when it approaches to the surface of the structure. The second component is sourced by the distortion of the wave which caused by the structure.

The latter problem, radiation, involves the calculation of the forces which represent the transferred energy to the fluid due to the oscillations of the floating body with the effect of the incident waves. In order to calculate these motions of the floating body in waves, the added mass and hydrodynamic damping should also be calculated in addition to wave exciting forces. These two terms are covered within the context of the radiation problem.

In practice, two methods are commonly used to calculate the hydrodynamic loads: These are the strip theory and 3D panel method. In both methods similar theories are used. In strip method, the corresponding floating structure is divided into sections and the loads are calculated on these sections. After that, the solution on each section is integrated over the ship length. In 3D panel method, the structure is discretized by panel elements. The hydrodynamic solutions are carried out through these panels and integrated over the wetted surface.

2.1 Linear seakeeping theory

The sea waves and the motions in these waves have non-linear characteristics in nature. Formulation of the mathematical model of this complex problem is not a straightforward task but an important simplification can still be made by using potential theory. The fluid flow around the floating body can be linearized by potential theory which provides great convenience for the solution of seakeeping problem. The fluid flow is represented as a potential function and non-linear effects are simply ignored. Due to similar reasons, the linear wave theory is used to define the wave form.

The calculations are performed in frequency domain due to simplicity of solution and usage of linear theories. Based on the assumption of linear wave theory, sinusoidal harmonic waves were generated and these waves excite the floating body with the actual wave frequency. After that, the floating body oscillates for six degrees of freedom in complex harmonic form at the wave frequency (Figure 2-1). These motions occur in translation (surge, sway, heave) and rotation (roll, pitch, yaw). The wave length is assumed to be much larger than the amplitude of the wave. Therefore, the motions of the body are assumed to have small amplitudes.

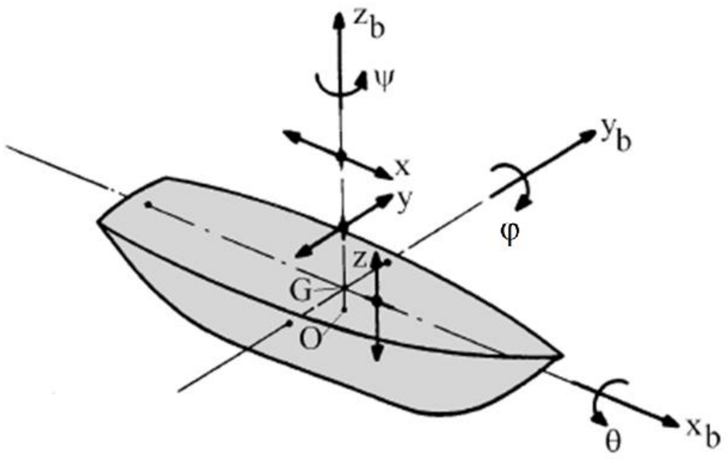

Figure 2-1: Degree of freedom of a ship (Journee and Massie, 2001)

The wavelengths are as long as the floating body’s length while the depth of fluid is much greater than the corresponding wave length. Therefore it is assumed that the depth is infinite and shallow water effects are negligible. In addition, the elastic deformation caused by the wave loads on floating body is neglected and it is assumed that the body is rigid.

Ignoring the viscous effects may cause inaccurate results for prediction of the resonance frequency of roll motion. In order to take the viscous effects into account, roll damping coefficient is introduced with empirical formulations (Journée and Adegeest, 2003).

2.1.1 Linear wave theory and potential flow

Waves have complex characteristics in a viscous fluid. Viscous effects are often concentrated on the surface and on a thin boundary layer at the bottom. Some simplifications can be made in practical engineering applications. In linear wave theory it is assumed that the fluid is ideal in definition of small amplitude waves. This means that the density in every point of the fluid is the same, incompressible and irrotational. In addition to these, the viscosity and the surface tension are neglected.

According to the potential theory, the velocity of the flow can be calculated in any point of the fluid domain by a potential function. The velocity components at one desired point are calculated by taking appropriate derivatives of potential function, (ϕ). In order to obtain this, the inlet fluid mass should be the equal to the outlet fluid mass in a closed control volume according to the conservation of mass. Based on this principle, the conservation of mass equation or *continuity equation* can be written as in (2.1).

$$\frac{\partial u_x}{\partial x}+\frac{\partial u_y}{\partial y}+\frac{\partial u_z}{\partial z}=0 \qquad \text{continuity equation} \qquad (2.1)$$

where u represents velocity of the fluid and x, y, z represents the direction of the velocity.

Solution of the continuity equation can be achieved by using a velocity potential function $\phi=\phi(x,y,z,t)$. This function is defined as the partial differential of the velocity of the water particles. If we write Eq. (2.1) in terms of velocity potential (2.2), the Laplace Equation (2.3) will be derived.

$$\text{Velocity potential function:} \qquad u_x=\frac{\partial \phi}{\partial x}, \quad u_y=\frac{\partial \phi}{\partial y}, \quad u_z=\frac{\partial \phi}{\partial z} \qquad (2.2)$$

$$\text{Laplace equation:} \qquad \frac{\partial^2 \phi}{\partial x^2}+\frac{\partial^2 \phi}{\partial y^2}+\frac{\partial^2 \phi}{\partial z^2}=0 \qquad (2.3)$$

Regarding the potential theory, in order the velocity potential to have the same value on any point of the fluid, ϕ =constant, the velocity potential should satisfy the Laplace Equation defined in (2.3). Also, the kinematic boundary conditions should satisfy on sea surface and sea bottom in addition to the equation of continuity.

$$\text{Kinematic boundary condition} \qquad \begin{array}{l} \text{on bottom: } \dfrac{\partial \phi}{\partial z}=0\text{ , z = -d} \\ \text{on surface: } \dfrac{\partial \phi}{\partial z}=\dfrac{\partial z}{\partial t}\text{ , z = 0} \end{array} \qquad (2.4)$$

2.1.2 Dynamics of floating bodies

A floating body is excited by two different forces while going in inviscid regular waves. The first one is the hydrostatic restoring force and the other one is hydrodynamic force caused by incident waves. As shown in Figure 2-2, total hydrodynamic forces can be obtained by calculation of the wave excitation forces and inertial & damping forces caused by the motion of the floating body.

First, the incident wave forces are obtained by the calculation of dynamic pressure on the wetted surface area. Total dynamic pressure is defined based on the linearized Bernoulli equation and the corresponding forces are obtained by integrating the pressure along the wetted surface. The inertial (including added mass) and damping forces can be calculated after the radiation potential is obtained. A detailed description about the subject will be given in the following sections. Also, hydrostatic restoring forces are calculated based on dynamic pressure.

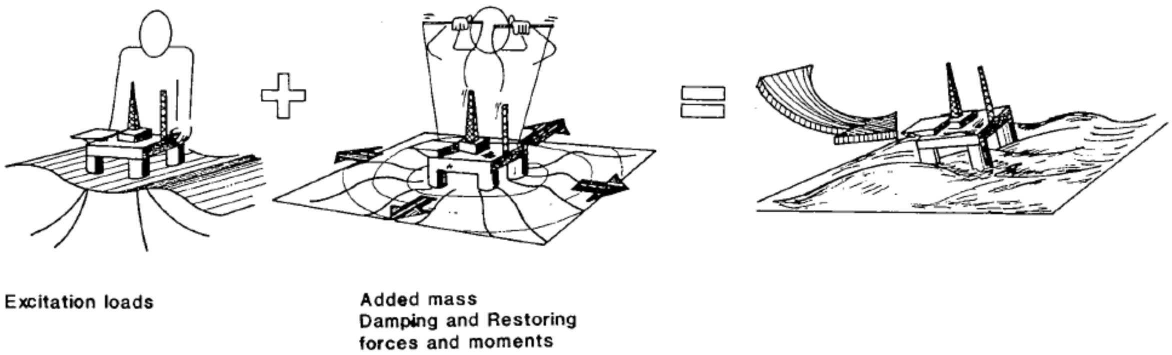

Figure 2-2 : Superposition of wave excitation, added mass, damping and restoring loads (Faltinsen, 1990)

The velocity potential of the fluid around the floating body is defined as in (2.5).

$$\Phi(x,y,z,t) = \zeta_a \phi(x,y,z) e^{-i\omega_e t} \tag{2.5}$$

where ζ_a represents compelling wave amplitude, ω_e represents encounter frequency.

The encounter frequency is defined as:

$$\omega_e = \omega - \frac{\omega^2 U}{g}\cos\mu \tag{2.6}$$

The term $\phi(x, y, z)$ related to the position in the equation can be divided into incident potential, diffraction potential and radiation potential which is caused by the oscillation of body in six degree of freedom. All these three potentials have complex characters.

The translational and rotational motions of the body in the unit amplitude regular incident waves can be written as:

$$x_j = u_j,\ (j = 1,2,3)$$
$$x_j = \theta_{j-3},\ (j = 4,5,6)$$

Total potential is composed of incident, diffraction and radiation potentials:

$$\phi(x, y, z)e^{-i\omega t} = \left[(\phi_I + \phi_d) + \sum_{6}^{j=1}\phi_{rj}x_j\right]e^{-i\omega t} \tag{2.7}$$

where ϕ_I the first order incident wave is potential, ϕ_d is the diffraction wave potential and ϕ_{rj} is the radiation wave potential caused by jth motion.

Since the velocity potential of the wave is obtained, the first-order hydrodynamic pressure distribution (2.8) can be calculated utilizing the linearized Bernoulli equation.

$$p^{(1)} = \rho\left[i\omega_e\,\phi(x, y, z) + \vec{U}\,\nabla\phi(x, y, z)\right]e^{-i\omega_e t} \tag{2.8}$$

Forces induced by waves can be calculated by integration of pressure on wetted surface. To represent the forces and moments in general form, the unit normal vector is defined in six degree of freedom as below:

$$
\begin{aligned}
\left(n_1, n_3, n_3\right) &= \vec{n} \\
\left(n_4, n_5, n_6\right) &= \vec{r} \, x \, \vec{n}
\end{aligned}
$$

where $\vec{r} = \vec{X} - \vec{X}_g$ represents the position vector. It is the location of any point on wetted surface according to the structure’s center of gravity.

First order hydrodynamic forces and moments are expressed by below general formula with this notation:

$$
F_j e^{-i\omega t} = -\int_{S_0} p^{(1)} n_j dS = -\rho \int_{S_0} \left[\left(i\omega_e + \vec{U} . \nabla \right) \phi(x, y, z) \right] n_j dS \tag{2.9}
$$

where S_0 represents the wetted surface of the structure.

From equation (2.10), the total first order hydrodynamic forces are written as below:

$$
F_j = \left[\left(F_{Ij} + F_{dj} \right) + \sum_{k=1}^{6} F_{rjk} x_k \right] \quad j = 1, 6 \tag{2.10}
$$

j[th] Froude-Krylov force due to incident wave:

$$F_{Ij} = -\rho \int_{S_0} \left[\left(i\omega_e + \vec{U}.\nabla \right) \phi_I \left(x, y, z \right) \right] n_j dS \tag{2.11}$$

j[th] diffraction force due to diffracted wave:

$$F_{dj} = -\rho \int_{S_0} \left[\left(i\omega_e + \vec{U}.\nabla \right) \phi_d \left(x, y, z \right) \right] n_j dS \tag{2.12}$$

j[th] radiation force due to unit amplitude rigid motion of k[th]:

$$F_{rjk} = -\rho \int_{S_0} \left[\left(i\omega_e + \vec{U}.\nabla \right) \phi_{rk} \left(x, y, z \right) \right] n_j dS \tag{2.13}$$

2.1.2.1 Calculation of Added Mass and Radiation Damping

The radiated waves are caused by oscillation of the floating body in still water (Fang et al, 2014). Radiated waves are strongly related to the hydrodynamic characteristics of the body. Therefore, real and imaginary parts of the radiation potential ϕ_{rk} are used in order to calculate the added mass and damping of the body in induced wave frequency. By also using (2.13), added mass (2.14) is proportional to the acceleration of the motion and damping (2.15) is proportional to the velocity of the motion.

$$A_{jk} = \frac{\rho}{\omega_e^2} \iint_{S_0} \mathrm{Re} \left[\left(i\omega_e + \vec{U}.\nabla \right) \phi_{rk} \left(x, y, z \right) \right] n_j dS \tag{2.14}$$

$$B_{jk} = -\frac{\rho}{\omega_e} \iint_{S_0} \mathrm{Im} \left[\left(i\omega_e + \vec{U}.\nabla \right) \phi_{rk} \left(x, y, z \right) \right] n_j dS \tag{2.15}$$

2.1.3 Kinematics of floating bodies

Floating bodies have linear and harmonic motions response under harmonic waves. Rigid motions in six DOF are associated with each other. These motions are expressed mathematically by general formulation of equation of motion in (2.16) (Salvesen et al, 1970).

$$\sum_{k=1}^{6}\left[\left(M_{jk}+A_{jk}\right)\ddot{\eta}_k+B_{jk}\,\dot{\eta}_k+C_{jk}\,\eta_k\right]=F_j e^{i\omega t}\ ;\ j=1,..,6 \tag{2.16}$$

Where M_{jk} represents generalized mass matrix:

$$M_{jk}=\begin{pmatrix} M & 0 & 0 & 0 & M_{zc} & 0 \\ 0 & M & 0 & -M_{zc} & 0 & 0 \\ 0 & 0 & M & 0 & 0 & 0 \\ 0 & -M_{zc} & 0 & I_4 & 0 & I_{46} \\ M_{zc} & 0 & 0 & 0 & I_5 & 0 \\ 0 & 0 & 0 & -I_{46} & 0 & I_6 \end{pmatrix} \tag{2.17}$$

A_{jk} represents added mass and B_{jk} represents damping matrix:

$$A_{jk}(\text{or } B_{jk})=\begin{pmatrix} A_{11} & 0 & A_{13} & 0 & A_{15} & 0 \\ 0 & A_{22} & 0 & A_{24} & 0 & A_{26} \\ A_{31} & 0 & A_{33} & 0 & A_{35} & 0 \\ 0 & A_{42} & 0 & A_{44} & 0 & A_{46} \\ A_{51} & 0 & A_{53} & 0 & A_{55} & 0 \\ 0 & A_{62} & 0 & A_{46} & 0 & A_{66} \end{pmatrix} \tag{2.18}$$

C_{jk} represents the hydrostatic restoring matrix. . Hydrostatic restoring forces are the forces when the structure returns to static position while moving in waves and independent of wave frequencies (Salvesen et al, 1970). For floating bodies, the structure is tended to return only in heave, pitch and roll motion. Therefore, the restoring forces for these motions are written as below:

$$C_{33} = \rho g A \tag{2.19}$$

$$C_{44} = \rho g A_{xx} + M g (z_b - z_G) = \rho g V GM_T \tag{2.20}$$

$$C_{55} = \rho g A_{yy} + M g (z_b - z_G) \tag{2.21}$$

$$C_{35} = C_{53} = -\rho g A_y \tag{2.22}$$

where ρ is density, g is gravitational acceleration, A is waterline area, A_y is first moment of inertia of waterline area, A_{xx} and A_{yy} are second moment of inertia of waterline area, V is volumetric displacement of floating body, z_b is the position of center of buoyancy and z_G is the position of center of gravity.

The most general form of the equation of motion, given in equation (2.16), should be solved simultaneously in order to consider the effects of all the motion to each other. However, by assuming lateral symmetry for a marine vessel the interconnecting six equations of motion can be converted into two independent equation sets. Therefore interconnecting six equations of motion can be converted into two independent equation sets. The first equation set is being established for surge, heave and pitch and the other can be set up for sway, roll and yaw. Both sets of equations are independent of one another due to the lateral symmetry. Thus, the coupled system can be represented by an appropriate uncoupled system.

Although it is not applicable to all ships together, the order of the hydrodynamic forces induced by surge motion is relatively insignificant compared to other motions for long and slender ships. Therefore in first set of equation, the heave (2.23) and pitch (2.24) are assessed together (Salvesen et al, 1970).

$$\left(M + A_{33}\right)\ddot{\eta}_3 + B_{33}\dot{\eta}_3 + C_{33}\eta_3 \quad + \quad A_{35}\ddot{\eta}_5 + B_{35}\dot{\eta}_5 + C_{35}\eta_5 = F_3 e^{i\omega t} \tag{2.23}$$

$$A_{53}\ddot{\eta}_3 + B_{53}\dot{\eta}_3 + C_{53}\eta_3 \quad + \quad \left(I_5 + A_{55}\right)\ddot{\eta}_5 + B_{55}\dot{\eta}_5 + C_{55}\eta_5 = F_5 e^{i\omega t} \tag{2.24}$$

2.1.3.1 Definition of RAO (Response Amplitude Operator)

After obtaining solutions for the equations of motion, motions of the floating body can be achieved. The amplitude and phase of response given by the floating body in regular waves can be defined with RAO (Response Amplitude Operator) or transfer functions for unit amplitude wave excitation. When the general equation of motion (2.16) is re-formed, RAO for each frequency can be written as equation (2.25).

$$RAO(\omega) = \frac{\eta_k}{\zeta_a} = \frac{F}{\sqrt{\left[C - \left(M + A(\omega)\right)\omega^2\right]^2 + \left(iB(\omega)\omega\right)^2}} \tag{2.25}$$

RAO curves give information about motion characteristics of floating body in calculated frequency range. The hydrostatic restoring force is more dominant in regions where the oscillation frequency (ω) of the structure is smaller than the natural frequency (ω_n) for that motion ($\omega < \omega_n$), which can also be understood from a typical RAO curve shown in Figure 2-3. The amplitude of the motion will be approximately the same with amplitude of the wave when the frequency goes to zero. The area, where the oscillation frequency and natural frequency approach to each other ($\omega \cong \omega_n$), is the most critical situation for the structure. The damping forces are effective in this region and especially the structure experience excessive motion relatively to wave amplitude. In the region, where oscillation frequency is larger than the natural frequency ($\omega > \omega_n$), the mass term is dominant. In this case the motions of the structure have relatively less magnitude while considering other conditions.

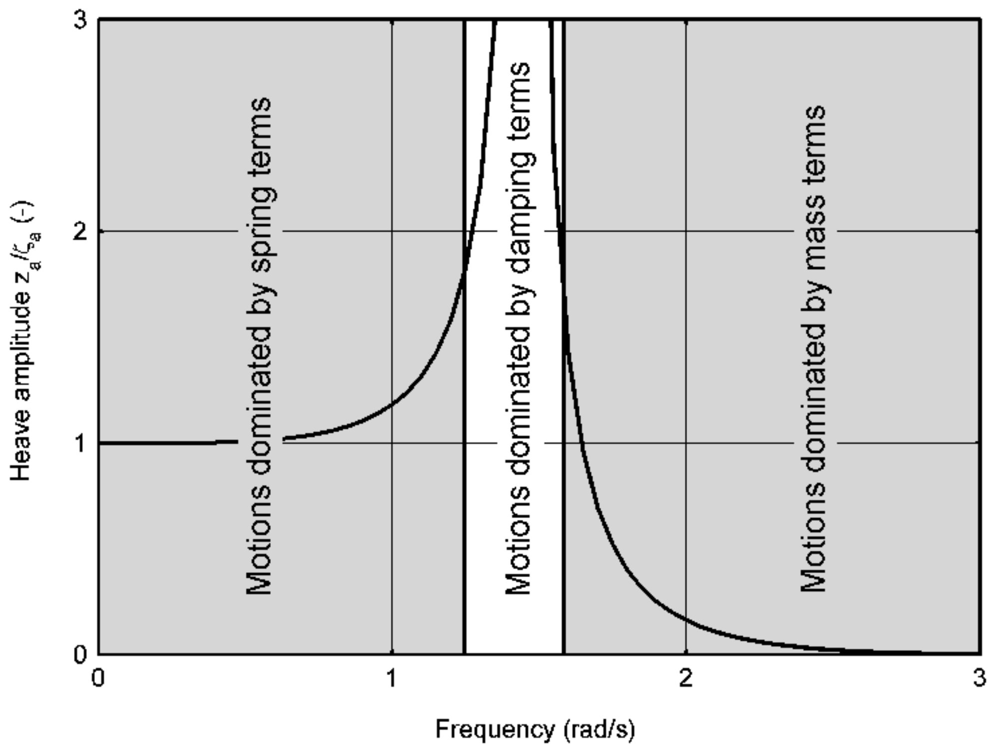

Figure 2-3 : Frequency areas of motion characteristics (Journee and Massie, 2001)

2.1.4 Strip theory

Strip theory is based on the calculation of three dimensional fluid forces using two dimensional potential theory. According to Korvin-Kroukovsky (1961), "the strip theory has been introduced in order to replace a three-dimensional hydrodynamic problem by a summation of two-dimensional ones. Using this method, solutions are possible for a much wider range of problems and actual hydrodynamic conditions connected with ship motions can be represented more completely." The first researcher to introduce the strip approach was Lewis (1929) but, Korvin-Kroukovsky and Jacobs (1957) applied the theory for prediction of ship motion for the first time. Later the theory has been modified and extended. Most of today's strip methods are variations of the strip method proposed by Salvesen, Tuck and Faltinsen (1970).

Strip theory is commonly used for seakeeping calculations in practice. The method is founded on the discretization of the ship into 2-D segments (generally 20-30) and solutions are performed on these segments. Then each solution is integrated along the ship length. Thus, this three dimensional physical phenomena can be defined by two dimensional boundary value data set.

While the floating body is divided into two dimensional rigid closed sections in finite number, the formulation also considers the physical and mathematical effects of each section to each other. As shown in Figure 2-4 the obtained sections are assumed to be a cylinder which has infinite length.

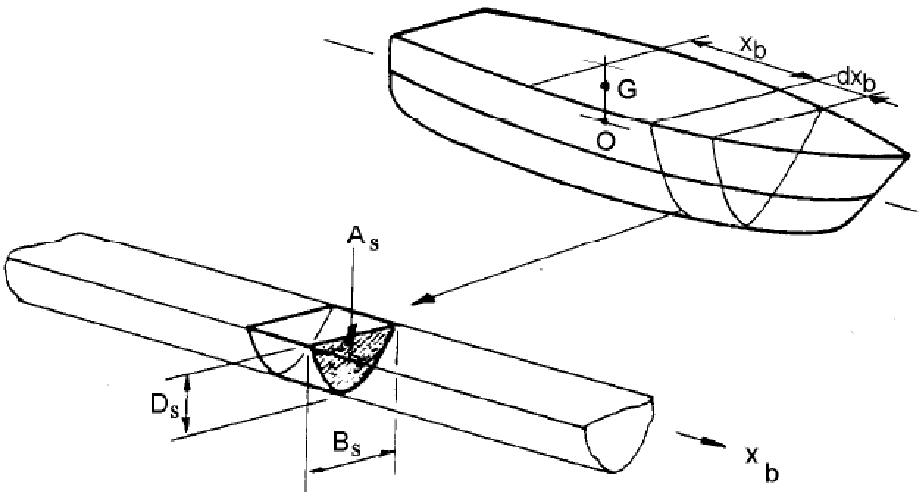

Figure 2-4 : Segment approach for the strip theory (Journee and Massie, 2001)

The first studies on the strip theory were made in the 1950s. The flow around the formal cylinder is defined with two dimensional potential theory and the hydrodynamic equations were solved by Ursell (1949).

Tasai (1959) developed a method which is called Lewis transformation. The application of this method is very simple in a lot of cases but, less realistic to transform ship-like cross sections to this unit circle to Ursell's solution.

Finally, in order to model the ship sections more realistic, the Frank-Close Fit method, which is used quite commonly and is based on the distribution of the singularity onto the ship sections, has been developed by Frank (1967).

Strip theory suits well for long and slender shaped ships (L>>B, T<<λ, B <<λ). The results diverge for the ships which have a ratio of L/B < 3.0. In addition, the strip theory is developed on the basis of linearity. The assumption is made such that the motion of the ship is smaller than the size of the ship sections. Hydrodynamic calculations are only performed for the ship’s hull area under the calm water line. In the case of wave loading, the margin of the errors can increase due to not taking into account the parts of the body under & above water line during the motion of the body. In addition, in high speed vessels or in extreme sea conditions the strip theory remains partially inadequate for high amplitude motions of the ships.

Despite all these limitations, the strip theory is used for seakeeping calculations because of giving fast and sufficiently accurate results in preliminary design stage of the ship.

2.1.5 Frank close-fit method

One of the most important part of the solution of equation of motion is determining the added mass and damping forces. As motioned in above, these forces are a part of radiation problem. Therefore, first, radiation potential must have to obtained.

In Frank Close-Fit method, the submerged ship section is divided into straight-line segments as shown in Figure 2-5. The velocity potential can be determined by distributing the sources over the submerged ship section. The density of these sources, which is unknown, can be found by Green functions which are satisfied boundary conditions in each segments. By using the linearized Bernoulli equation, the hydrodynamic pressures can be generated from the velocity potential. If these pressures are integrated along the submerged ship section, sectional added mass and damping coefficients can be obtained (Frank, 1967).

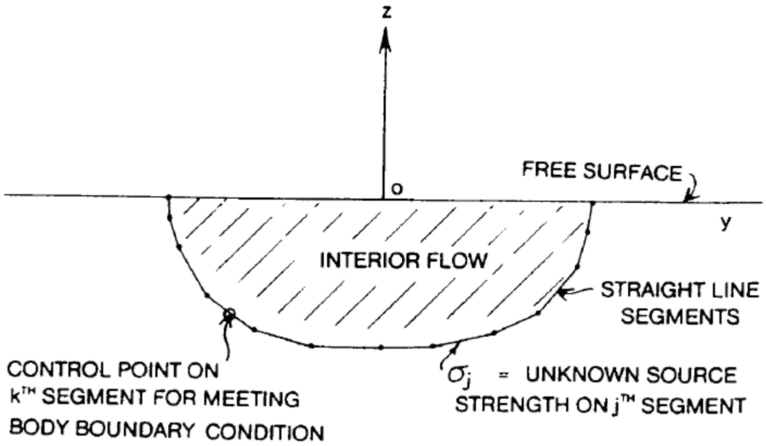

Figure 2-5: Sectional approximation for Frank's method (Beck et all., 1989)

Consider a cylinder which is partially immersed horizontally in infinite depth and C_0 is cross sectional counter in rest position as shown in Figure 2-5. The body is forced into simple harmonic motion, $A^{(m)}\cos(\omega t)$ by incident waves. Where ω is the frequency of oscillation and m=2,3,4 corresponding to sway, heave and roll motions.

The main objective is find a velocity potential (2.26) which is satisfying the boundary conditions:

$$\Phi^{(m)}(x,y,\mathrm{t}) = \mathrm{Re}\left[\phi^{(m)}(x,y)e^{-i\omega t}\right] \tag{2.26}$$

1) The Laplace equation which is given in Eq. (2.3)

2) The free surface or dynamic boundary condition :

$$\frac{\partial^2\phi}{\partial t^2} + g\frac{\partial\phi}{\partial z} = 0 \quad at\ z = 0 \tag{2.27}$$

The requirement for dynamic boundary condition (2.27) is that the pressure at the surface equals the atmospheric pressure.

3) The seabed boundary for deep water which is given in Eq. (2.4)

4) Kinematic boundary condition of oscillating body:

$$\frac{\partial \phi}{\partial n} = v_n(x, y, z, t) = \sum_{j=1}^{6} v_j f_j(x, y, z) \tag{2.28}$$

Kinematic boundary condition of oscillating body (2.28) is the boundary condition at the surface of the floating body and implies that the velocity of the water particles (v_n) at the surface of the floating body are equal to the velocity of the floating body (v_j) for six degree of motion (i=1…6).

5) Radiation condition:

$$\lim_{R \to \infty} \phi = 0 \tag{2.29}$$

The requirement for radiation condition (2.29) is far from the oscillating body the potential value has to become zero. To meet this requirement, the radiation condition states that at a large distance (R) from the floating body the potential value becomes zero.

6) Symmetric or Anti-symmetric condition:

$$\begin{aligned} \phi_2(-x, z) &= -\phi_2(+x, z) \quad \textit{Sway} \\ \phi_3(-x, z) &= +\phi_3(+x, z) \quad \textit{Heave} \\ \phi_4(-x, z) &= -\phi_4(+x, z) \quad \textit{Roll} \end{aligned} \tag{2.30}$$

Floating bodies are generally symmetric with respect to its middle line plane. Therefore, the potential equations can be reduced to Eq. (2.30). The indices represent the directions. The horizontal velocities, $\frac{\partial \phi}{\partial x}$, of the water particles have to be in the same direction. Therefore, sway and roll motions are anti-symmetric. Due to the horizontal velocities have opposite signs, heave motion is symmetric. The vertical velocities, $\frac{\partial \phi}{\partial y}$, must have the same direction on both sides at any time.

Let the Green function (2.31) which is satisfy the radiation (2.29) and seabed boundary condition (2.4):

$$
\begin{aligned}
G(z,\zeta) = \frac{1}{2}.\operatorname{Re}&\left\{\ln\left(z-\zeta\right) - \ln\left(z-\bar{\zeta}\right) + 2.PV\int_0^{\infty} \frac{e^{-i.k\left(z-\bar{\zeta}\right)}}{v-k}\,dk\right\} \\
&- i.\operatorname{Re}\left\{e^{-i.k\left(z-\bar{\zeta}\right)}\right\}
\end{aligned}
\tag{2.31}
$$

where ζ is complex variable along C_{0}.

The real point-source potential is:

$$
H\left(x,y,\xi,\eta,t\right) = \operatorname{Re}\left\{G\left(z,\zeta,t\right).e^{-i\omega t}\right\} \tag{2.32}
$$

Another expression satisfying all these condition is:

$$
H\left(x,y,\xi,\eta,t-\frac{\pi}{2\omega}\right) = \operatorname{Re}\left\{i.G\left(z,\zeta,t\right).e^{-i\omega t}\right\} \tag{2.33}
$$

By superposition of Eq. (2.32) and Eq. (2.33), the velocity potential is obtained:

$$\Phi^{(m)}(x,y,\mathrm{t}) = \mathrm{Re}\left[\int_{C_0} Q(s).G\left(z,\zeta\right)e^{-i\omega t}.ds\right] \tag{2.34}$$

where Q(s) is the complex source density as a function along C_0.

In Eq. (2.34), Q(s) is still unknown. To calculate the source density, the kinematic boundary condition on oscillating body (2.28) is applied:

$$\begin{aligned}
&\mathrm{Re}\left\{\left(\vec{n}.\vec{\nabla}\right).\int_{C_0} Q(s).G\left(z,\zeta\right)ds\right\} = 0\\
&\mathrm{Im}\left\{\left(\vec{n}.\vec{\nabla}\right).\int_{C_0} Q(s).G\left(z,\zeta\right)ds\right\} = A^{(m)}.\omega.n^{(m)}
\end{aligned} \tag{2.35}$$

where $n^{(m)}$ represents the direction cosine of the normal velocity at z on the cylinder.

With linearized Bernoulli equation, the hydrodynamic pressure can obtain in i-th midpoint of segment (x_i,y_i):

$$p^{(m)}(x_i,y_i,\omega,\mathrm{t}) = -\rho\frac{\partial\Phi^{(m)}}{\partial t}(x_i,y_i,\omega,\mathrm{t}) \tag{2.36}$$

$p^{(m)}$ is consist of two part which are $p_a{}^{(m)}$, hydrodynamic pressure in-phase with the displacement and $p_v{}^{(m)}$, hydrodynamic pressure in-phase with the velocity.

Calculation of $p^{(m)}$ for each segment over the cross section C_0 is summed for obtaining sectional added mass ($M^{(m)}$) and damping ($N^{(m)}$) forces or moments:

$$M^{(m)} = 2.\sum_{i=1}^{N}\left\{p_a{}^{(m)}(x_i, y_i, \omega, \mathrm{t})n_i{}^{(m)}.\left|s_j\right|\right\} \tag{2.37}$$

$$N^{(m)} = 2.\sum_{i=1}^{N}\left\{p_v{}^{(m)}(x_i, y_i, \omega, \mathrm{t})n_i{}^{(m)}.\left|s_j\right|\right\} \tag{2.38}$$

3. SOLUTION OF LINEAR SEAKEEPING PROBLEMS BY AQWA

ANSYS AQWA software is an engineering analysis suite of tools for the investigation of the effects of wave, wind and current on floating and fixed offshore and marine structures, including spars, floating production storage and offloading (FPSO) systems, semi-submersibles, tension leg platforms (TLPs), ships, renewable energy systems and breakwater design (AQWA, 2013).

3.1 Assumptions in AQWA

ANSYS-AQWA can calculate the wave loads by using 3D panel method and linear 3D potential theory. In 3D panel method, first the structure is discretized into panels and the singularities used for solutions of boundary value problems are distributed over panels which represent the wetted surface. For the final result, the hydrodynamic solutions performed over panels are integrated along the wet surface (AQWA, 2013).

In order this theory to be applicable, it is also assumed that the depth is infinite and the diffraction and radiation problems are solved in frequency domain. The fluid is considered as ideal. The fluid is assumed that the viscous forces are negligible. Also, it is incompressible and irrotational.

To predict the motions in sea waves, the fluid forces as shown in Figure 3-1 are calculated at first. Hydrostatic force is independent of wave frequency. Therefore, it can be calculated directly by vessel characteristics. Hydrodynamic forces can be calculated by the total potential, which is given in Eq. (2.7). As it is mentioned before, the total potential consists of incident, diffraction and radiation potentials. In order to obtain the incident force (see Eq. (2.11)) and diffraction force (see Eq.(2.12)), incident and diffraction potential are employed.

In Eq. (2.16), the equation of motion for harmonic motion response is defined. Also, Eq. (2.25) is employed to predict RAOs for each frequency.

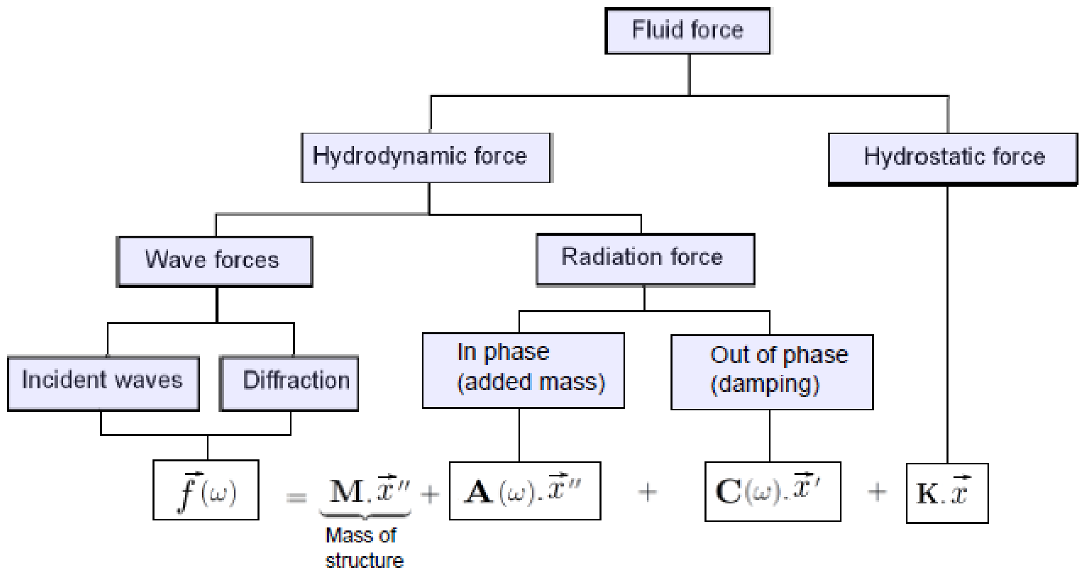

Figure 3-1: Summary of fluid force (ANSYS, 2014)

3.2 Source distribution method

A boundary integration approach is employed in AQWA to solve the fluid velocity potential governed by the below boundary conditions. In this approach the frequency domain Green's function in finite depth water is introduced, which obeys the same linear free surface boundary condition, seabed condition, and far field radiation conditions as those given in (2.27) and (2.4) (AQWA, 2013).

1) The Laplace equation which is given in Eq. (2.3)

2) The free surface or dynamic boundary condition in Eq. (2.27)

3) The seabed boundary for deep water which is given in Eq. (2.4)

4) Kinematic boundary condition of oscillating body which is given in Eq. (2.28)

In additionally Eq. (2.28), Eq. (3.1) must satisfy for diffraction potential.

$$\frac{\partial \phi}{\partial n} = -\frac{\partial \phi_I}{\partial n} \tag{3.1}$$

5) Radiation condition which is given in Eq. (2.29)

Using Green's theorem, the velocity potential of diffraction and radiation waves can be expressed as in Eq. (3.2).

$$c\phi\left(\vec{X}\right) = \int_{S_0} \left\{ \phi\left(\vec{\zeta}\right) \frac{\partial G(\vec{X},\vec{\zeta},\omega)}{\partial n\left(\vec{\zeta}\right)} - G(\vec{X},\vec{\zeta},\omega) \frac{\partial \phi\left(\vec{\zeta}\right)}{\partial n\left(\vec{\zeta}\right)} \right\} dS \tag{3.2}$$

where

$$\mathrm{c} = \begin{cases} 0 & \vec{X} \notin \Omega \cup S_0 \\ 2\pi & \vec{X} \in S_0 \\ 4\pi & \vec{X} \in \Omega \end{cases} \qquad \Omega : \text{Fluid domain}$$

$\vec{X} = (X, Y, \mathrm{Z})$ is the location of a point on the submerged body surface.

S_0 is submerged body surface.

$\vec{\zeta} = (\xi, \eta, \zeta)$ denotes the position of a source.

The source distribution over the mean wetted surface, the fluid potential is given in Eq. (3.3).

$$\phi\left(\vec{X}\right) = \frac{1}{4\pi} \int_{S_0} \sigma\left(\vec{\zeta}\right) G(\vec{X},\vec{\zeta},\omega)\, dS \quad \text{where } \vec{X} \in \Omega \cup S_0 \tag{3.3}$$

where $\sigma\left(\vec{\zeta}\right)$ is unknown source strength.

To obtain the source strength over the mean wetted surface, kinematic boundary condition of oscillating body given in Eq. (2.28) can be applied:

$$\frac{\partial \phi\left(\overrightarrow{X}\right)}{\partial n\left(\overrightarrow{X}\right)} = -\frac{1}{2}\sigma\left(\overrightarrow{X}\right) + \frac{1}{4\pi}\int_{S_0} \sigma\left(\vec{\zeta}\right)\frac{\partial G(\overrightarrow{X},\vec{\zeta},\omega)}{\partial n\left(\overrightarrow{X}\right)} dS \qquad \text{where } \overrightarrow{X} \in S_0 \tag{3.4}$$

where n is the normal vector of the hull.

To solve the above equation, in which the mean wetted surface of a floating body is divided into quadrilateral or triangular panels in AQWA. It is assumed that the potential and the source strength within each panel are constant and taken as the corresponding average values over that panel surface. The discrete integral form (3.3) and (3.4):

$$\begin{aligned} &\phi\left(\overrightarrow{X}\right) = \frac{1}{4\pi}\sum_{m=1}^{N_p}\sigma_m G(\overrightarrow{X},\overrightarrow{\zeta_m},\omega)\,\Delta S_m \qquad \text{where } \overrightarrow{X} \in \Omega \cup S \\ &-\frac{1}{2}\sigma_k + \frac{1}{4\pi}\sum_{m=1}^{N_p}\sigma_m \frac{\partial G(\overrightarrow{X_k},\overrightarrow{\zeta_m},\omega)}{\partial n\left(\overrightarrow{X_k}\right)}\Delta S_m = \frac{\partial \phi\left(\overrightarrow{X_k}\right)}{\partial n\left(\overrightarrow{X_k}\right)} \quad \text{where } \overrightarrow{X} \in S_0, k = 1, N_p \end{aligned} \tag{3.5}$$

where N_p is the total number of the panels over the mean wetted body surface, ΔS_m is the area of the m-th panel, $\overrightarrow{\zeta_m}$ and $\overrightarrow{X_k}$ are the coordinates of panel geometric center over the *m*-th and *k*-th panels respectively.

After obtaining the diffraction and radiation potential, hydrodynamic pressure can be calculated by using the linearized Bernoulli’s equation which is given in Eq. (2.8).

Integration of the pressure along wetted surface lets to calculate hydrodynamic forces and moments as given in Eq. (2.9).

Also, added mas and damping can be expressed in real and imaginary parts of radiation potential as given Eq. (2.14) and Eq. (2.15)

3.3 Multi-body diffraction analysis

The software provides an integrated environment for developing the primary hydrodynamic parameters required for undertaking complex motions and response analyses. Three-dimensional linear radiation and diffraction analysis may be undertaken with multiple bodies (Figure 3-2), taking full account of hydrodynamic interaction effects that occur between bodies.

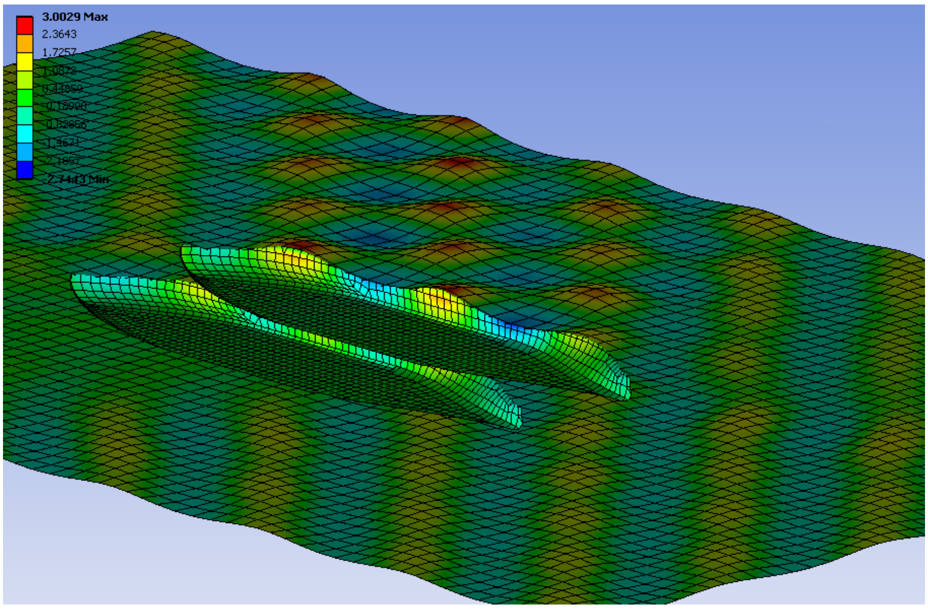

Figure 3-2 : Demonstration of multiple body solution in AQWA (ANSYS, 2014)

Fixed bodies such as breakwaters or gravity-based structures may be included in the models. Computation of the second-order wave forces via the full quadratic transfer function matrices permits use over a wide range of water depths. User-defined stiffness matrix definition enables mooring and connection systems to be included in the diffraction analysis where these significantly impact the motions response of the structures. ANSYS AQWA can also generate pressure and inertial loading for use in a structural analysis as part of the vessel hull design process (Figure 3-3).

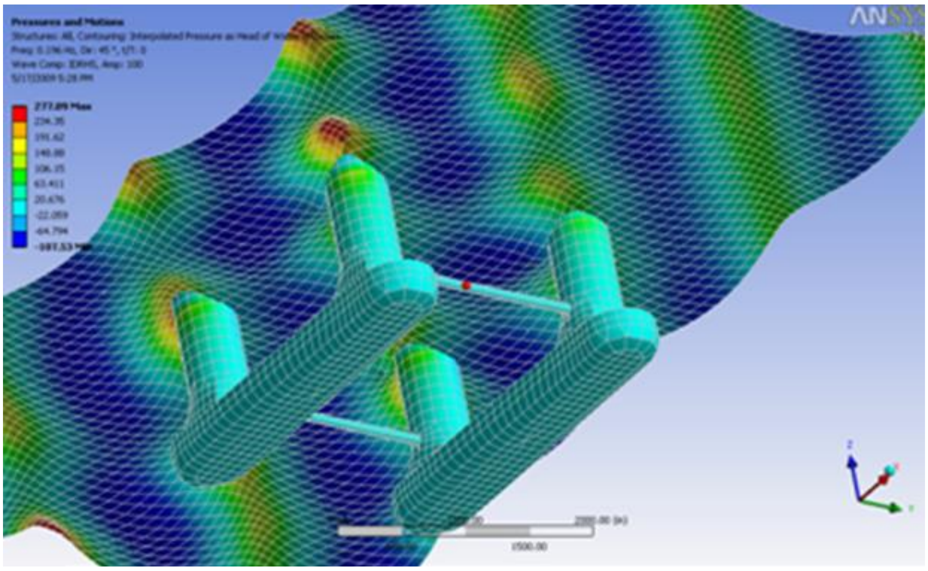

Figure 3-3 : Hydrodynamics pressure on a semi-submersible (ANSYS, 2014)

3.4 Hydrodynamic pressure mapping for structural analysis

The results from a diffraction analysis can be mapped onto an ANSYS structural mechanics product for further structural assessment and detailed design (Figure 3-4). Since the mapping function automatically accounts for mesh differences between the hydrodynamic and finite element models they do not have to be topologically identical.

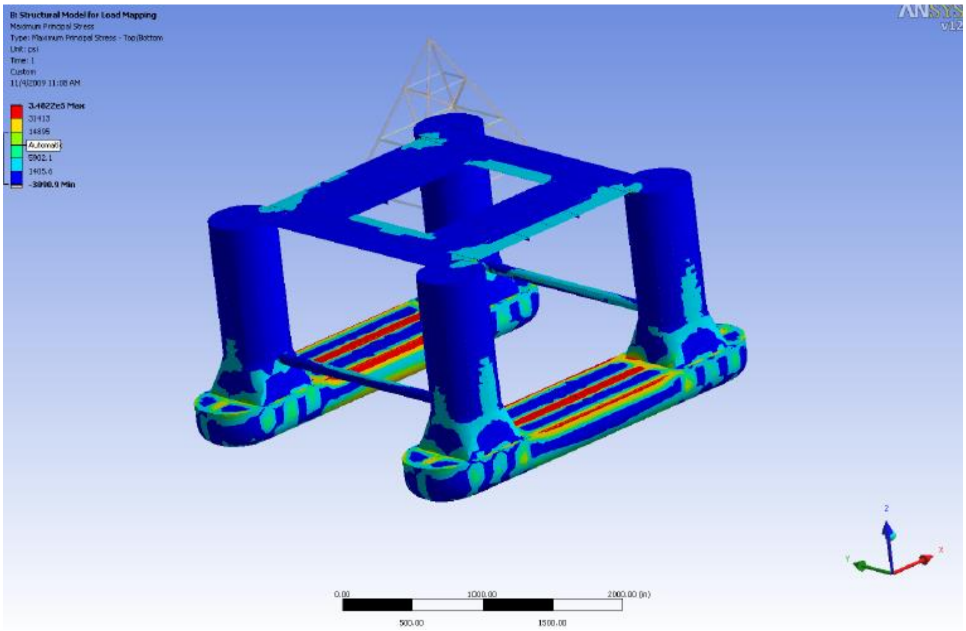

Figure 3-4 : Hydrodynamic pressure mapping for structural analysis (ANSYS, 2014)

3.5 Global hydrodynamic analysis

The generic nature of the program enables the hydrodynamic simulation of all types of offshore and marine structures including spars; floating production, storage and offloading (FPSO) vessels; semi-submersibles and ships. Specialized tether elements permit idealization of tension leg platforms while inclusion of bending stiffness in the mooring definition enables improved modeling of rigid and flexible risers.

3.6 Frequency and time-domain options

The ANSYS AQWA provides the flexibility to undertake simulations in either frequency or time domains, thus combining the speed of frequency-domain solutions for screening and initial studies with rigorous and more general time-domain capabilities. Slow-drift effects and extreme-wave conditions may be investigated within the time domain, and damage conditions, such as line breakage, may be included to investigate any transient effects that may occur.

4. VALIDATION STUDIES

In this section four studies are presented for validation of linear strip theory.

In the first study, two dimensional experimentally determined hydrodynamic coefficients of floating bodies having rectangular, triangular and cylindrical cross sections are compared with the results of AQWA analysis.

For later study, the seakeeping analysis of a barge having regular rectangular cross section is performed by using strip theory and AQWA. Then the results are compared.

The experimental results of heave and pitch motions of a Series 60 formed ship are compared with the results of AQWA analysis for the next study.

In the last study, the experimental results for the heave and pitch motions and vertical accelerations of a DTMB 5145 model representing the DDG51 type US Navy Combatant at speeds corresponding to Fn=0 and Fn=0.41, are compared with AQWA results.

4.1 Comparison of experimental results of hydrodynamics coefficients of rectangular, triangular and cylindrical shaped floating bodies with 3D panel method

In this study, the experimental and theoretical results of hydrodynamics coefficients of rectangular, triangular and cylindrical shaped floating bodies by Vugts (1968) are compared with AQWA analysis. The experimental results are dimensionless so that 3D AQWA results are converted to 2D via dividing the result by model length and non-dimensional form. The analysis data are non-dimensionalized as follows:

$$\mathbf{A_{33}} = \frac{a_{33}}{\rho A}, \ \mathbf{B_{33}} = \frac{b_{33}}{\rho A}\sqrt{\frac{B}{2g}}$$

where A_{33} and B_{33} are added mass and damping force, $a_{33} = \frac{A_{33}}{L}$ and $b_{33} = \frac{B_{33}}{L}$ represent added mass and damping coefficients results.

4.1.1 Rectangular shaped analysis and results

The dimensions of rectengular shaped floating body are given as below:

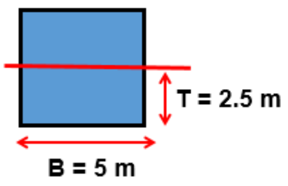

$A = 12.5\ m^2$ (sectional wetted surface area)

$B = 5$ m

$g = 9.8065\ m/s^2$

$\rho = 1.025\ ton/m^3$

The AQWA analysis is performed with model length, L = 25 m and panel model is discretized with 6492 elements of which 3246 elements are on the wetted surface (Figure 4-1).

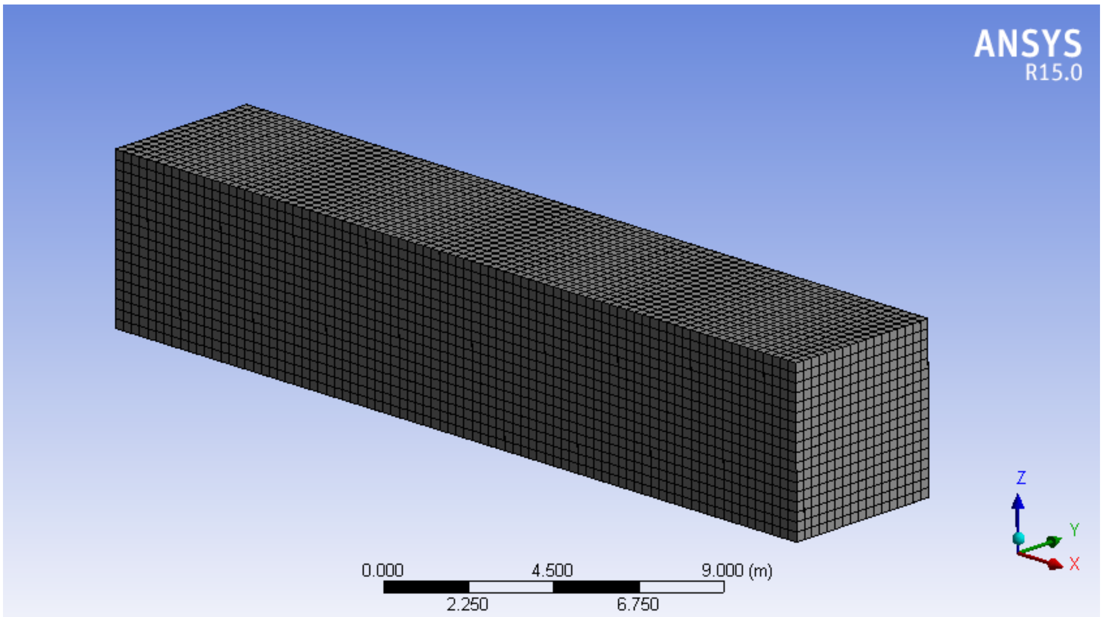

Figure 4-1 : The panel model of rectangular shaped floating body

Added mass and damping results of analysis, which is performed in AQWA, is presented in Table 4-1.

Table 4-1 : Hydrodynamics coefficient for rectangular shaped floating body–AQWA result

ω	A_{33} (ton)	B_{33} (kN/(m/s))	$\omega\sqrt{\frac{B}{2g}}$	$\frac{a_{33}}{\rho A}$	$\frac{b_{33}}{\rho A}\sqrt{\frac{B}{2g}}$
0.150	534.924	2.558	0.076	1.670	0.004
0.332	545.743	25.554	0.168	1.704	0.040
0.414	538.212	45.091	0.209	1.680	0.071
0.426	536.379	48.379	0.215	1.675	0.076
0.439	534.174	52.082	0.222	1.668	0.082
0.453	531.506	56.265	0.229	1.659	0.089
0.514	517.588	75.070	0.260	1.616	0.118
0.696	456.995	134.585	0.351	1.427	0.212
0.878	386.165	182.313	0.443	1.206	0.287
1.060	321.931	205.225	0.535	1.005	0.323
1.242	273.358	196.850	0.627	0.853	0.310
1.424	249.372	160.076	0.719	0.779	0.252
1.606	248.151	117.629	0.811	0.775	0.185
1.788	255.964	83.994	0.903	0.799	0.132
1.970	264.730	57.329	0.995	0.826	0.090
2.152	273.804	35.671	1.087	0.855	0.056
2.334	283.206	21.604	1.178	0.884	0.034
2.516	289.835	14.508	1.270	0.905	0.023
2.698	301.249	1.473	1.362	0.940	0.002
2.880	304.821	2.060	1.454	0.952	0.003
3.062	308.207	1.496	1.546	0.962	0.002
3.244	311.211	0.976	1.638	0.972	0.002
3.426	313.832	0.554	1.730	0.980	0.001
3.608	316.059	0.296	1.822	0.987	0.000
3.790	317.954	0.145	1.914	0.993	0.000
3.972	319.585	0.058	2.005	0.998	0.000
4.154	320.994	0.017	2.097	1.002	0.000
4.336	322.300	0.185	2.189	1.006	0.000
4.518	323.188	0.076	2.281	1.009	0.000
4.700	323.252	0.055	2.373	1.009	0.000

According to the experimental values and AQWA analysis, the non-dimensional a_{33} results for rectangular shaped floating body are presented in **Figure 4-2**.

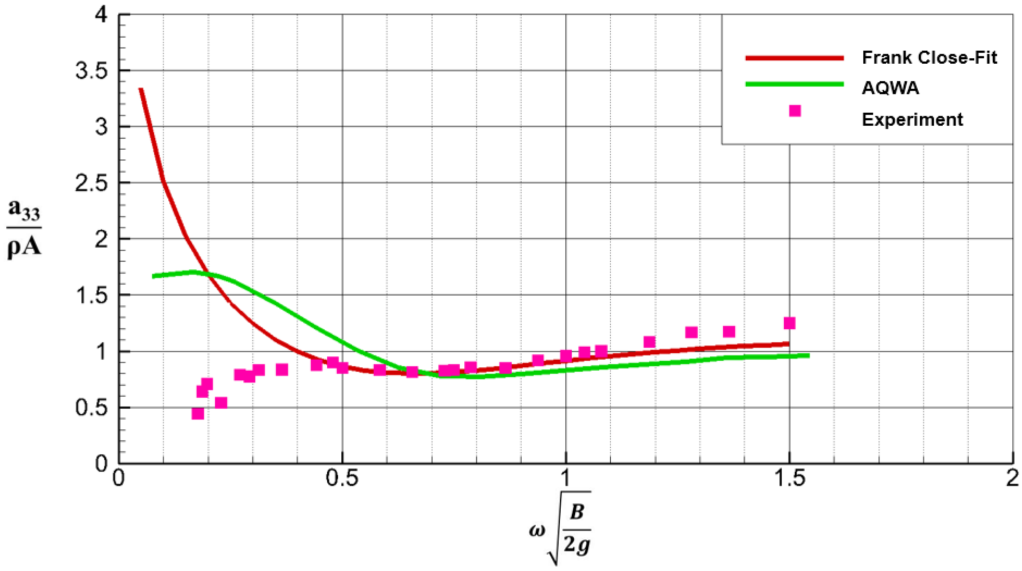

Figure 4-2 : Heave added mass coefficient results for rectangular shaped floating body

According to the experiment and AQWA analysis, the non-dimensional b_{33} results for rectangular shaped floating body are presented in Figure 4-3.

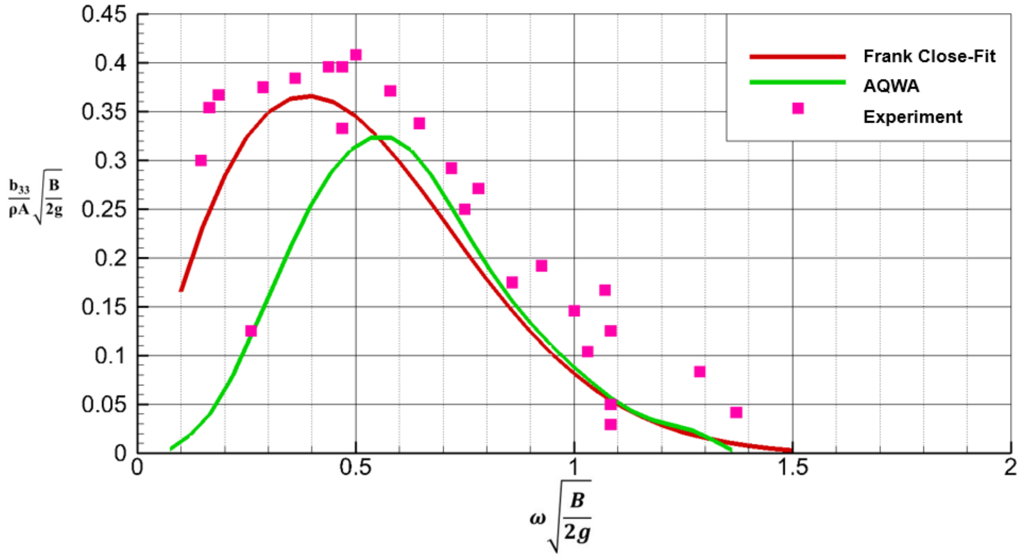

Figure 4-3 : Heave damping coefficient results for rectangular shaped floating body

4.1.2 Cylindrical shaped analysis and results

The dimensions of cylindrical shaped floating body are given as below:

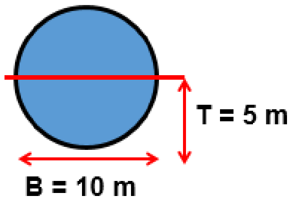

A = 39.27 m^2 (sectional wetted surface area)

B = 10 m

g = 9.8065 m/s^2

ρ = 1.025 ton/m^3

The AQWA analysis is performed with model length, L = 50 m and panel model is discretized with 22480 elements (Figure 4-4) of which 22480 elements are on wetted surface area.

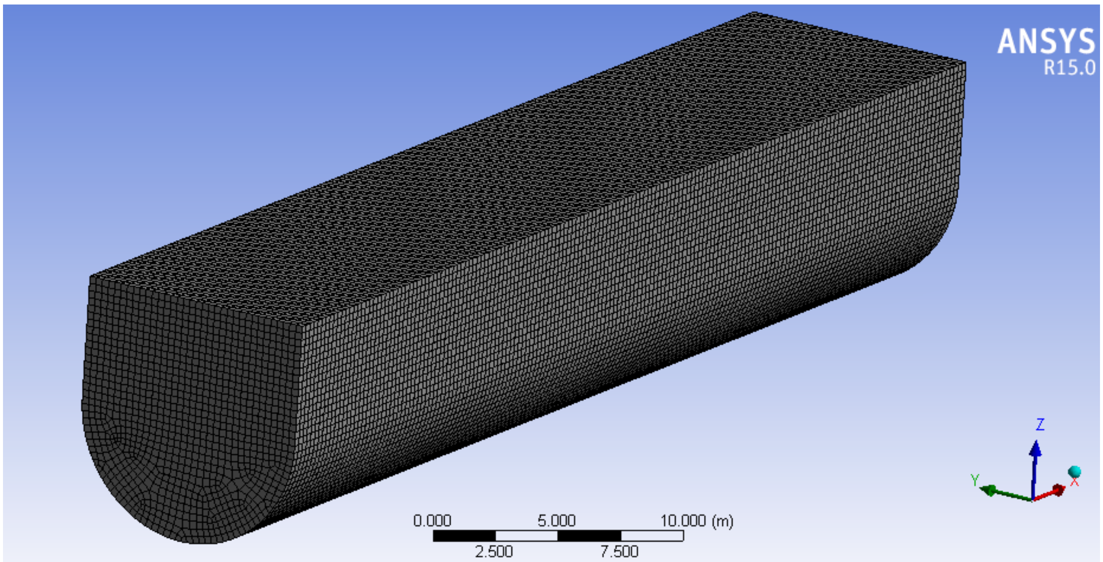

Figure 4-4 : The panel model of cylindrical shaped floating body

Added mass and damping coefficient values for AQWA analysis are presented in Table 4-2.

Table 4-2 : Hydrodynamics coefficient for cylindrical shaped floating body – AQWA result

ω	A_{33} (ton)	B_{33} (kN/(m/s))	$\omega\sqrt{\frac{B}{2g}}$	$\frac{a_{33}}{\rho A}$	$\frac{b_{33}}{\rho A}\sqrt{\frac{B}{2g}}$
0.150	3931.622	40.165	0.107	1.954	0.014
0.332	3886.648	362.114	0.237	1.931	0.128
0.514	3275.646	902.761	0.367	1.628	0.320
0.696	2477.781	1367.215	0.497	1.231	0.485
0.878	1769.211	1574.802	0.627	0.879	0.559
1.060	1332.966	1441.519	0.757	0.662	0.511
1.242	1214.321	1185.422	0.887	0.603	0.421
1.424	1201.237	977.773	1.017	0.597	0.347
1.606	1203.846	759.072	1.147	0.598	0.269
1.788	1261.119	562.283	1.277	0.627	0.199
1.970	1375.271	414.318	1.407	0.683	0.147
2.152	1430.835	309.859	1.537	0.711	0.110
2.334	1481.984	227.372	1.667	0.736	0.081
2.516	1529.831	169.309	1.797	0.760	0.060
2.698	1572.622	125.278	1.927	0.781	0.044
2.880	1608.982	92.742	2.056	0.799	0.033
3.062	1635.690	40.642	2.186	0.813	0.014
3.244	1665.323	53.532	2.316	0.827	0.019
3.426	1683.680	41.206	2.446	0.837	0.015
3.608	1691.356	33.094	2.576	0.840	0.012
3.790	1689.201	29.677	2.706	0.839	0.011
3.972	1690.579	2.631	2.836	0.840	0.001
4.154	1701.545	11.783	2.966	0.845	0.004
4.336	1709.220	11.869	3.096	0.849	0.004
4.518	1716.438	12.460	3.226	0.853	0.004
4.700	1722.120	0.787	3.356	0.856	0.000

According to the experimental values and AQWA analysis, the non-dimensional a33 results for cylindrical shaped floating body are presented in Figure 4-5.

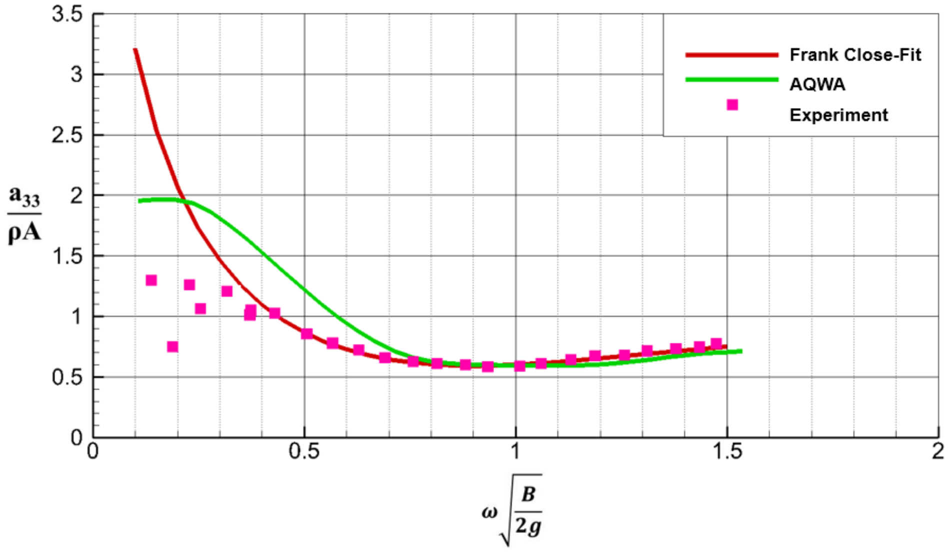

Figure 4-5 : Heave added mass coefficient results for cylindrical shaped floating body

Similarly, the non-dimensional b_{33} results for cylindrical shaped floating body are compared in Figure 4-6.

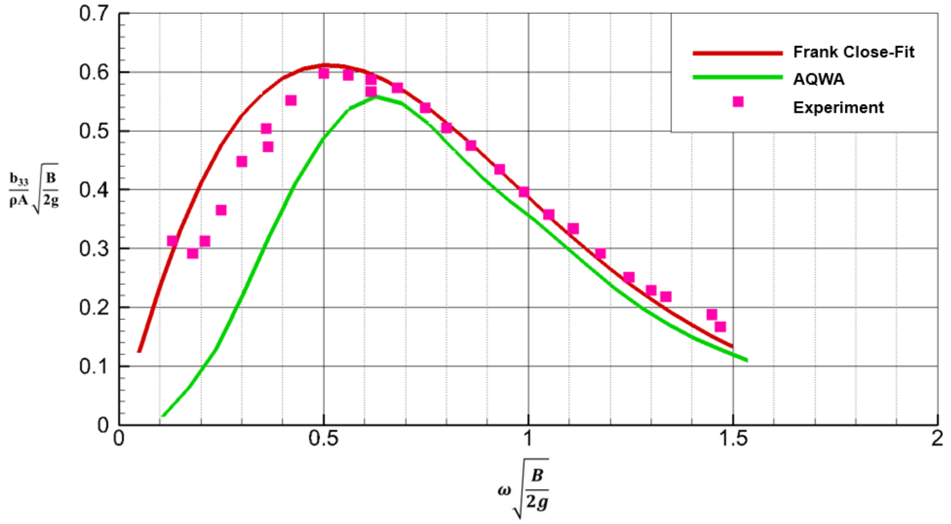

Figure 4-6 : Heave damping coefficient results for cylindrical shaped floating body

4.1.3 Triangular shaped analysis and results

The dimensions of triangular shaped floating body are

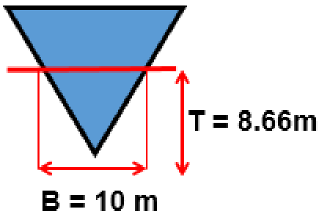

A = 43.301 m^2 (sectional wetted surface area)

B = 10 m

g = 9.8065 m/s^2

ρ = 1.025 ton/m^3

The AQWA analysis is performed with model length, L = 25 m and panel model is represented by 1846 elements (Figure 4-7) of which 888 elements are on the wetted surface area.

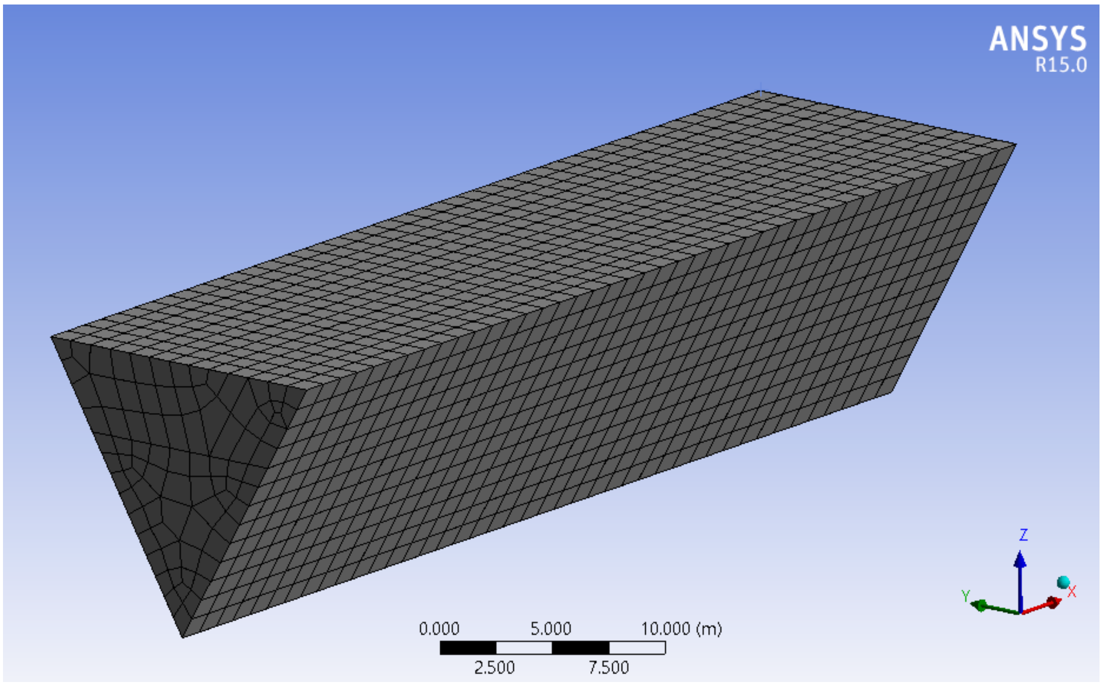

Figure 4-7 : The panel model of cylindrical shaped floating body

Added mass and damping coefficients determined with AQWA analysis are presented in Table 4-3.

Table 4-3 : Hydrodynamics coefficient for triangular shaped floating body – AQWA result

ω	A_{33} (ton)	B_{33} (kN/(m/s))	$\omega\sqrt{\frac{B}{2g}}$	$\frac{a_{33}}{\rho A}$	$\frac{b_{33}}{\rho A}\sqrt{\frac{B}{2g}}$
0.150	3583.409	40.197	0.107	1.615	0.013
0.238	3647.497	154.147	0.170	1.644	0.050
0.326	3565.140	348.039	0.233	1.607	0.112
0.414	3340.130	601.935	0.295	1.505	0.194
0.502	3014.188	878.225	0.358	1.358	0.283
0.590	2640.958	1141.924	0.421	1.190	0.367
0.678	2261.507	1369.934	0.484	1.019	0.441
0.766	1897.774	1547.981	0.547	0.855	0.498
0.853	1561.913	1661.208	0.609	0.704	0.535
0.941	1274.169	1693.307	0.672	0.574	0.545
1.029	1063.137	1647.887	0.735	0.479	0.530
1.117	935.793	1559.475	0.798	0.422	0.502
1.205	869.994	1464.596	0.861	0.392	0.471
1.293	838.119	1382.506	0.923	0.378	0.445
1.381	816.696	1317.468	0.986	0.368	0.424
1.469	792.955	1255.536	1.049	0.357	0.404
1.557	768.585	1180.056	1.112	0.346	0.380
1.645	762.847	1102.990	1.174	0.344	0.355
1.733	778.388	1039.755	1.237	0.351	0.335
1.821	793.609	985.173	1.300	0.358	0.317
1.909	807.943	927.164	1.363	0.364	0.298
1.997	824.895	869.008	1.426	0.372	0.280
2.084	843.670	815.609	1.488	0.380	0.262
2.172	861.844	766.784	1.551	0.388	0.247
2.260	879.843	720.666	1.614	0.396	0.232
2.348	897.333	674.373	1.677	0.404	0.217
2.436	914.67681	636.8579	1.740	0.412	0.205
2.524	929.41800	595.6605	1.802	0.419	0.192
2.612	943.89313	561.2126	1.865	0.425	0.181
2.700	956.44500	529.2803	1.928	0.431	0.170

According to the experimental results and AQWA analysis, the non-dimensional a_{33} results for triangular shaped floating body are presented in **Figure 4-8**.

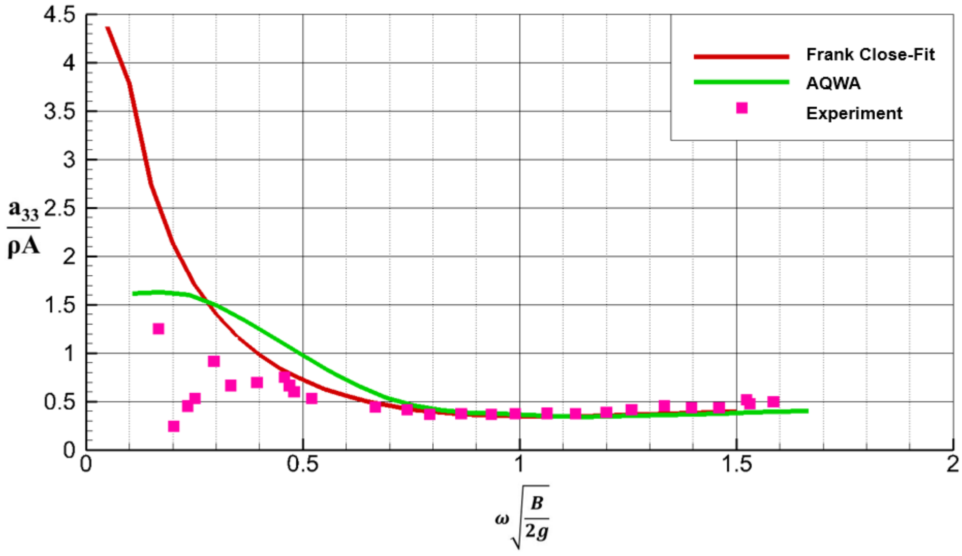

Figure 4-8 : Heave added mass coefficient results for triangular shaped floating body

Similarly, the non-dimensional a_{33} results for triangular shaped floating body are presented in Figure 4-9.

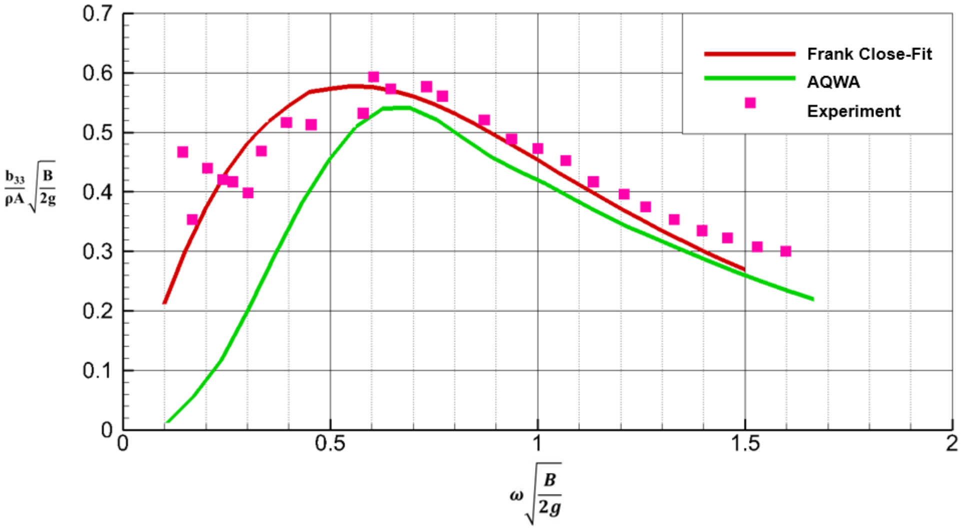

Figure 4-9 : Heave damping coefficient results for triangular shaped floating body

4.2 Comparison of the results of hydrodynamics coefficients, forces and motions of a barge in head seas with strip theory and 3D panel method

In this study, seakeeping calculations in head seas are performed with strip theory and ANSYS AQWA for the rectangular shaped barge whose dimensions are given in Table 4-4. The strip theory calculations are implemented with "BargeHead" software which is written in FORTRAN.

Table 4-4 : Main dimension of the barge

L =	200	m
B=	30	m
T =	15	m
D =	30	m

The strip theory calculations are performed for λ/L = 0.10, 0.20, 0.30, 0.40, 0.50, 0.60, 0.70, 0.80, 0.90, 1.00, 1.10, 1.20, 1.30, 1.40, 1.50, 1.60, 1.70, 1.80, 1.90, 2.00, 2.50, 3.00, 4.00, 5.00.

AQWA analysis is performed with respect to λ/L for the frequencies 0.24823, 0.27753, 0.32046, 0.35104, 0.39248, 0.40268, 0.41371, 0.4257, 0.43881, 0.4532, 0.4691, 0.48681, 0.50669, 0.52922, 0.55505, 0.58507, 0.62056, 0.66341, 0.71657, 0.78496, 0.87761, 1.01338, 1.24113, 1.75522 rad/s which are derived from (4.1).

$$k = \frac{2\pi}{\lambda} = \frac{\omega^2}{g} \quad \rightarrow \quad \omega = \sqrt{\frac{2\pi.g}{\lambda}} \tag{4.1}$$

4.2.1 General information about “BargeHead”

“BargeHead” is a FORTRAN code which can calculate complex vertical response of a barge in head seas. Main dimensions and sectional offsets of the barge are taken from a formatted text file. Subroutine TRAPEZ can calculate sectional area by Trapeze Method. Added mass and damping coefficients are calculated by subroutine FRANK. Subroutine SPL is a common function to obtain the whole model results from sections for example displacement and LCB of the barge, total exciting force/moment, added mass and damping forces. Complex vertical responses are calculated via subroutine VERMO.

4.2.2 AQWA model for the rectangular barge

Panel model used in ANSYS AQWA analysis is presented in Figure 4-10. The model consists of 8452 elements of which 4356 elements are diffracted (on wetted surface).

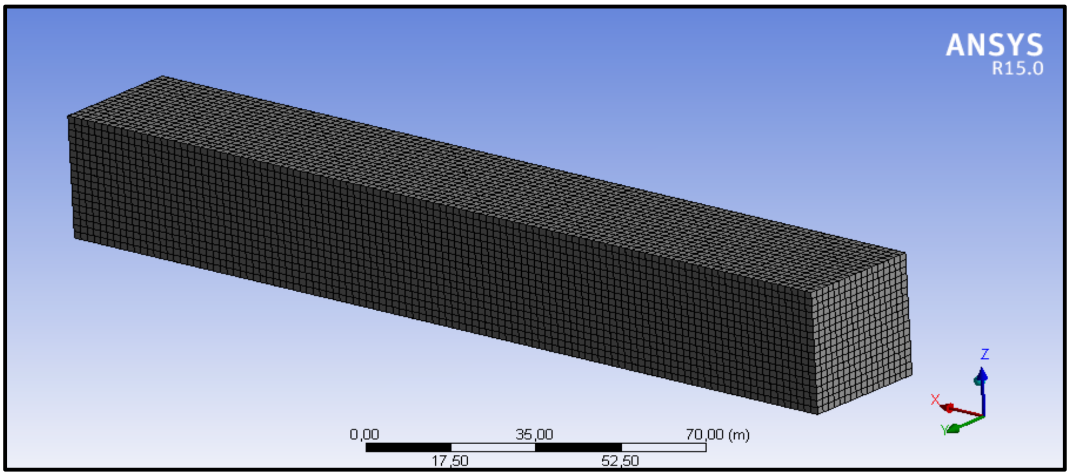

Figure 4-10 : Panel model of the barg

4.2.3 Hydrodynamic results for rectangular barge

The results for heave and pitch RAOs are presented in Figure 4-11 and Figure 4-12 respectively.

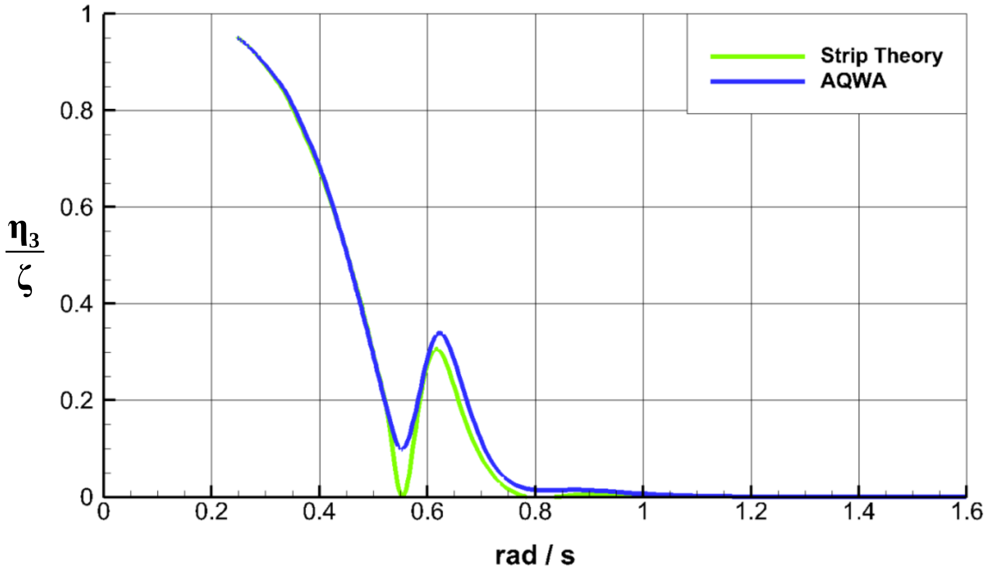

Figure 4-11 : Heave RAO for rectangular barge in head seas

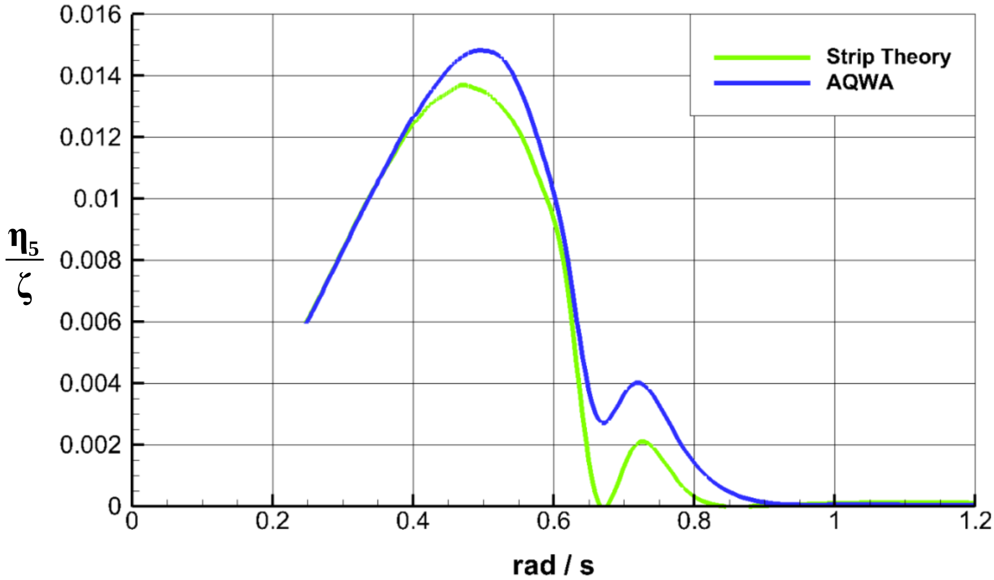

Figure 4-12 : Pitch RAO for rectangular barge in head seas

The results for total added mass and total radiation damping values are compared in Figure 4-13 and Figure 4-14 respectively.

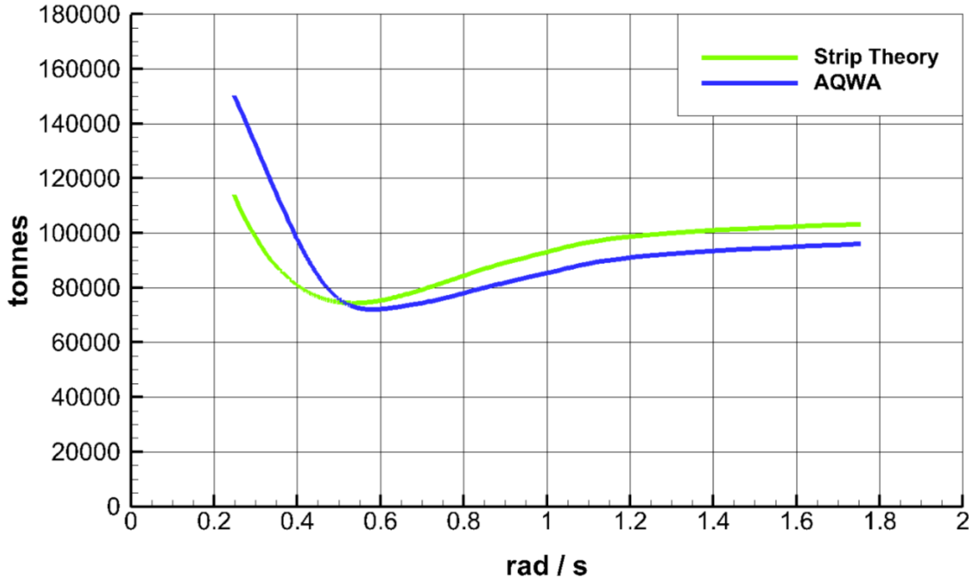

Figure 4-13 : Added mass for rectangular barge in head seas

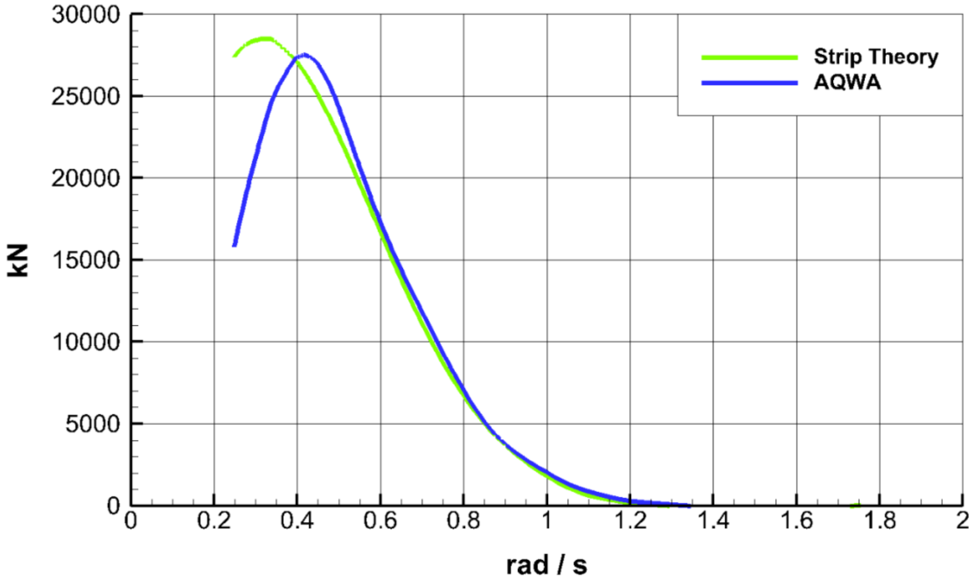

Figure 4-14 : Radiation damping for rectangular barge in head seas

Froude-Krylov and diffraction forces are compared in Figure 4-15 and Figure 4-16 respectively.

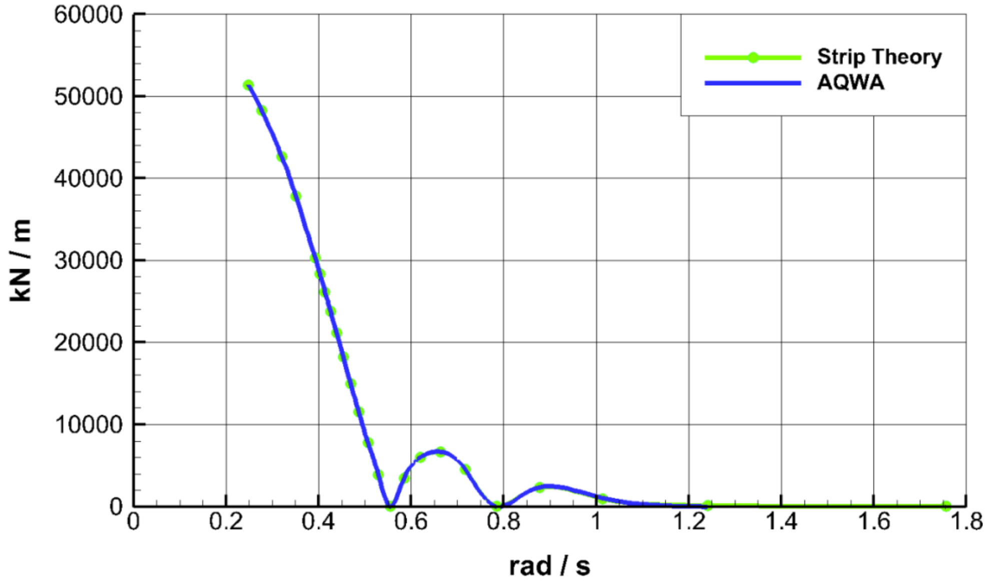

Figure 4-15 : Froude-Krylov force for rectangular barge in head seas

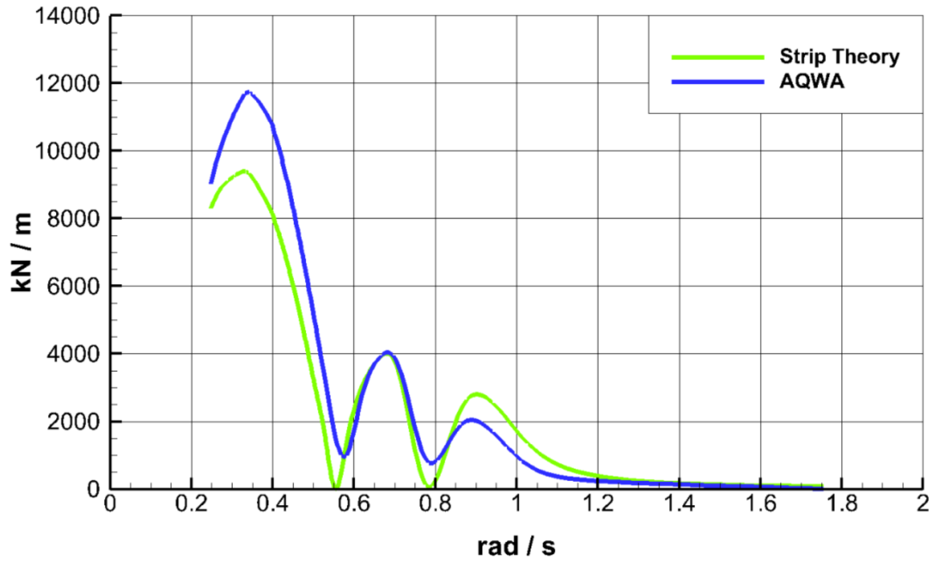

Figure 4-16 : Diffraction force for rectangular barge in head seas

Total exciting forces and moments are compared in Figure 4-17 and Figure 4-18 respectively.

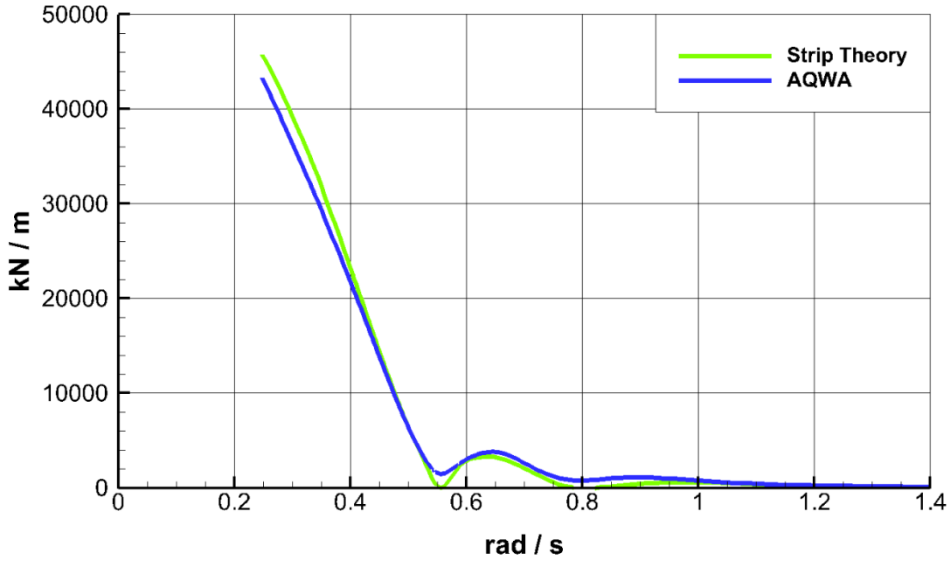

Figure 4-17 : Total exciting force for rectangular barge in head seas

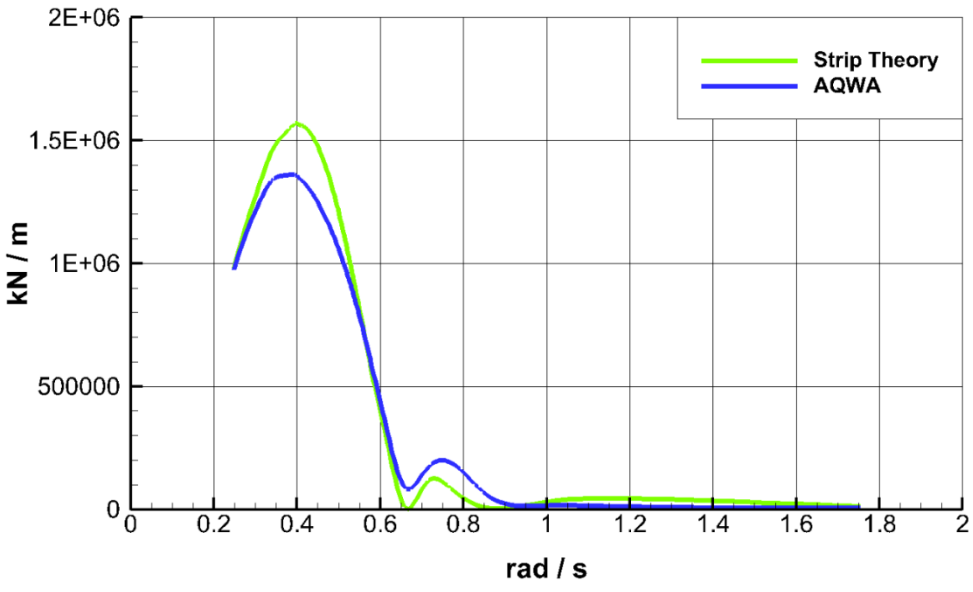

Figure 4-18 : Total exciting moment for rectangular barge in head seas

4.3 Comparison of experimental results of a Series 60 type ship heave and pitch motions with 3D panel method

In this study, the experimental results and strip theory calculations of a Series 60 formed ship with C_B=0.70 (Gerritsma and Beukelman, 1966) are compared with AQWA results for heave and pitch motions. The experiment was performed with wave height for $2\zeta_a/L_{BP}$=1/40 and 1/50.

4.3.1 Experimental model for Series 60

Main dimensions of model ship are presented in Table 4-5. In experiments, Fn=0.15 and Fn=0.20 cases are considered.

Table 4-5 : Main dimensions and radius of gyration of the ship for experiment

L_{BP} =	2.258	m
L_{WL} =	2.296	m
B =	0.322	m
T =	0.129	m
Volumetric displacement =	0.0657	m^3
C_B =	0.70	
C_M =	0.986	
C_P =	0.710	
A_W =	0.572	m^2
C_{WP} =	0.785	
LCB length =	0.011	from midship (+ fwd) m
k_{YY}, 0.25*L_{BP} =	0.574	m

4.3.2 AQWA model for Series 60

Main dimensions of AQWA model are presented in Table 4-6. The analyses are performed with 0.712 m/s forward speed for Fn=0.15 and 0.950 m/s forward speed for Fn=0.20 conditions.

Table 4-6 : Main dimensions and radius of gyration of the ship for AQWA

L_{BP} =	2.258	m
L_{WL} =	2.296	m
B =	0.322	m
T =	0.129	m
Volumetric displacement =	0.066	m^3
C_B =	0.7	
C_P =	0.71	
A_W =	0.572	m^2
C_{WP} =	0.787	
C_M =	0.986	
LCB length =	0.011	from midship (+ fwd) m
LCF length =	-0.038	from midship (+ fwd) m
k_{XX} ,0.34*B =	0.10948	m
k_{YY}, 0.25*L_{BP} =	0.574	m
k_{ZZ}, 0.26*L_{BP} =	0.59696	m

The AQWA analysis is performed with the panel model, which is presented in Figure 4-19. The model is discretized into 1596 elements of which 1116 are diffracted (on wetted surface).

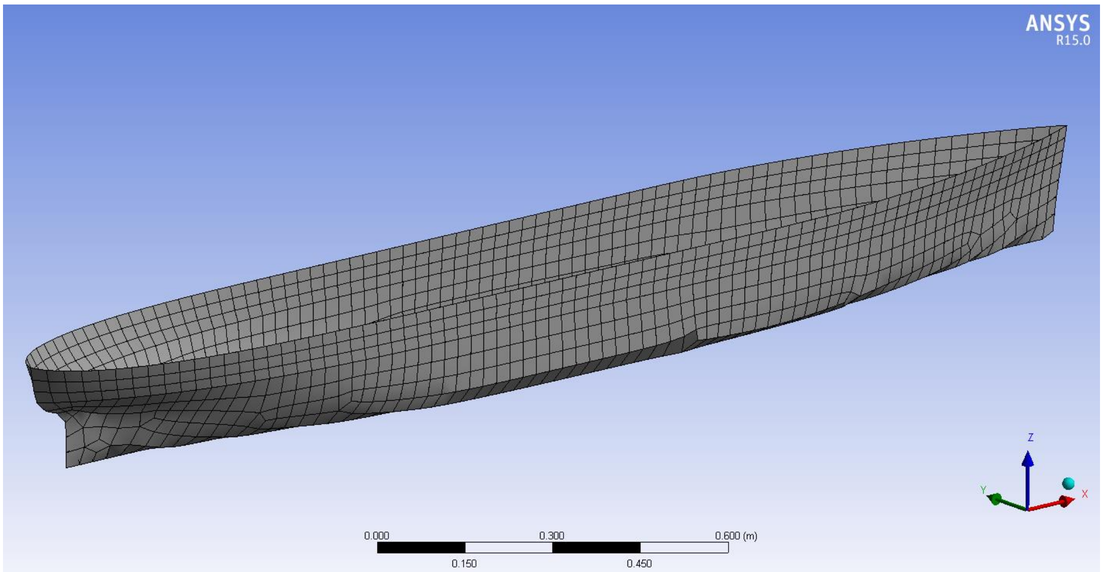

Figure 4-19 : The panel model for Series 60 form ship

4.3.3 AQWA motion results for Fn=0.15 condition

The results of heave and pitch analysis are presented in Table 4-7. The pitch results are non-dimensionalized by wave number, k.

Table 4-7 : AQWA heave and pitch results for Fn = 0.15

ω	λ / L_{BP}	Heave	Pitch	k	$\theta_a / k\xi_a$
3.8000	1.8904	0.8672	1.6390	1.4720	1.1135
3.9429	1.7559	0.8660	1.7759	1.5847	1.1206
4.0857	1.6353	0.8715	1.9005	1.7016	1.1168
4.2286	1.5266	0.8852	2.0123	1.8227	1.1040
4.3714	1.4285	0.9096	2.1152	1.9479	1.0859
4.5143	1.3395	0.9493	2.2153	2.0773	1.0664
4.6571	1.2586	1.0082	2.3152	2.2109	1.0472
4.8000	1.1848	1.0806	2.4054	2.3486	1.0242
4.9429	1.1173	1.1340	2.4556	2.4905	0.9860
5.0857	1.0554	1.1020	2.4110	2.6365	0.9145
5.2286	0.9985	0.9310	2.2143	2.7867	0.7946
5.3714	0.9461	0.6572	1.8699	2.9411	0.6358
5.5143	0.8977	0.3826	1.4651	3.0996	0.4727
5.6571	0.8530	0.1726	1.0861	3.2623	0.3329
5.8000	0.8115	0.0339	0.7674	3.4292	0.2238
5.9429	0.7729	0.0504	0.5111	3.6002	0.1420
6.0857	0.7371	0.0969	0.3117	3.7753	0.0826
6.2286	0.7036	0.1184	0.1637	3.9546	0.0414
6.3714	0.6724	0.1239	0.0681	4.1381	0.0165
6.5143	0.6433	0.1188	0.0695	4.3258	0.0161
6.6571	0.6160	0.1076	0.1129	4.5176	0.0250
6.8000	0.5903	0.0927	0.1444	4.7136	0.0306

The experimental values, strip theory and AQWA analysis results of Series 60 formed ship for Fn=0.15 heave and pitch motion are compared as shown in Figure 4-20 and Figure 4-21 respectively.

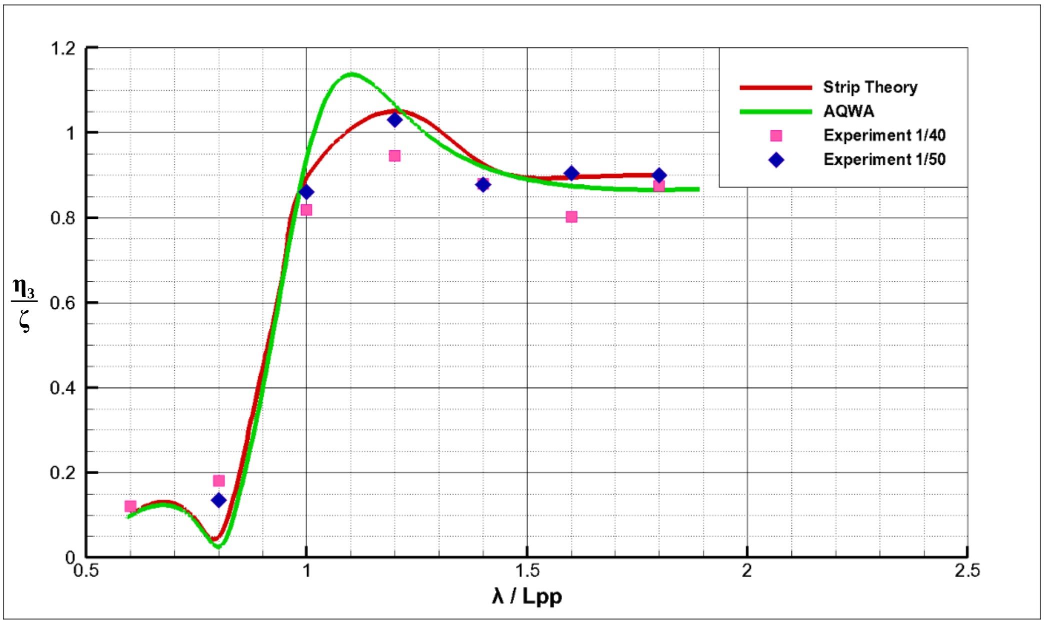

Figure 4-20 : Heave result Fn = 0.15

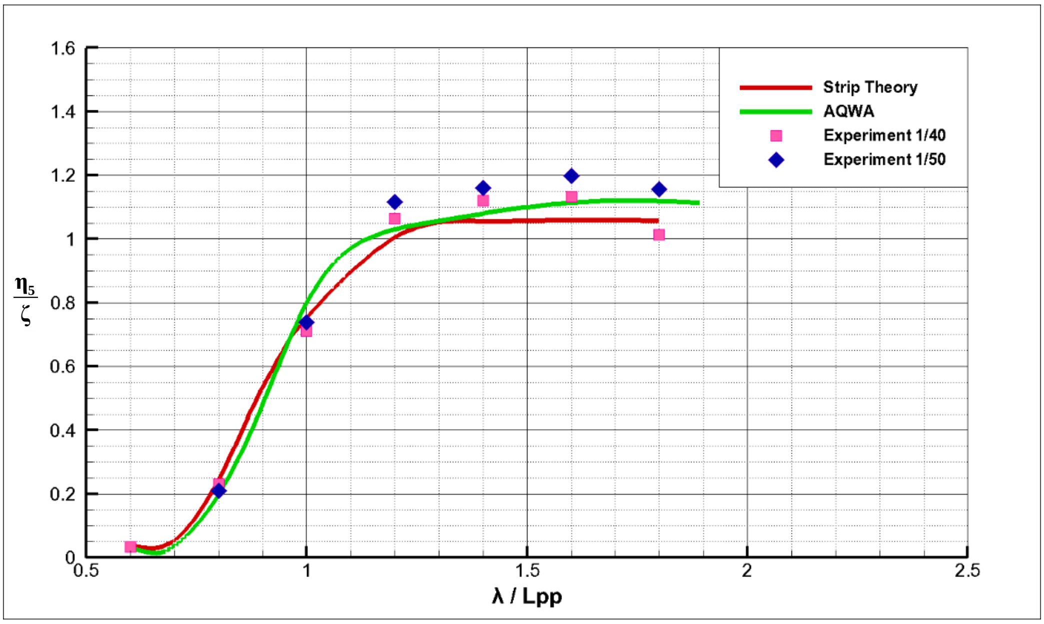

Figure 4-21 : Non-dimensional pitch result Fn = 0.15

4.3.4 AQWA motion results for Fn=0.20 condition

The results of heave and pitch analysis are presented in Table 4-8. Similar to Fn=0.15 condition, the pitch results are non-dimensionalized by wave number, k.

Table 4-8 : AQWA heave and pitch results for Fn = 0.20

ω	λ / L_{BP}	Heave	Pitch	k	$\theta_a / k\xi_a$
3.8000	1.8904	0.9721	1.7501	1.4720	1.1135
3.9429	1.7559	1.0067	1.8837	1.5847	1.1206
4.0857	1.6353	1.0570	2.0098	1.7016	1.1168
4.2286	1.5266	1.1296	2.1371	1.8227	1.1040
4.3714	1.4285	1.2323	2.2743	1.9479	1.0859
4.5143	1.3395	1.3643	2.4223	2.0773	1.0664
4.6571	1.2586	1.4913	2.5649	2.2109	1.0472
4.8000	1.1848	1.5234	2.6442	2.3486	1.0242
4.9429	1.1173	1.3535	2.5386	2.4905	0.9860
5.0857	1.0554	1.0032	2.1905	2.6365	0.9145
5.2286	0.9985	0.6364	1.7332	2.7867	0.7946
5.3714	0.9461	0.3575	1.3072	2.9411	0.6358
5.5143	0.8977	0.1717	0.9546	3.0996	0.4727
5.6571	0.8530	0.0570	0.6739	3.2623	0.3329
5.8000	0.8115	0.0317	0.4573	3.4292	0.2238
5.9429	0.7729	0.0662	0.2911	3.6002	0.1420
6.0857	0.7371	0.0861	0.1665	3.7753	0.0826
6.2286	0.7036	0.0935	0.0814	3.9546	0.0414
6.3714	0.6724	0.0923	0.0542	4.1381	0.0165
6.5143	0.6433	0.0857	0.0803	4.3258	0.0161
6.6571	0.6160	0.0757	0.1073	4.5176	0.0250
6.8000	0.5903	0.0638	0.1239	4.7136	0.0306

The experimental values, strip theory and AQWA analysis results of Series 60 formed ship for Fn=0.15 heave and pitch motion are compared as shown in Figure 4-22 and Figure 4-23 respectively.

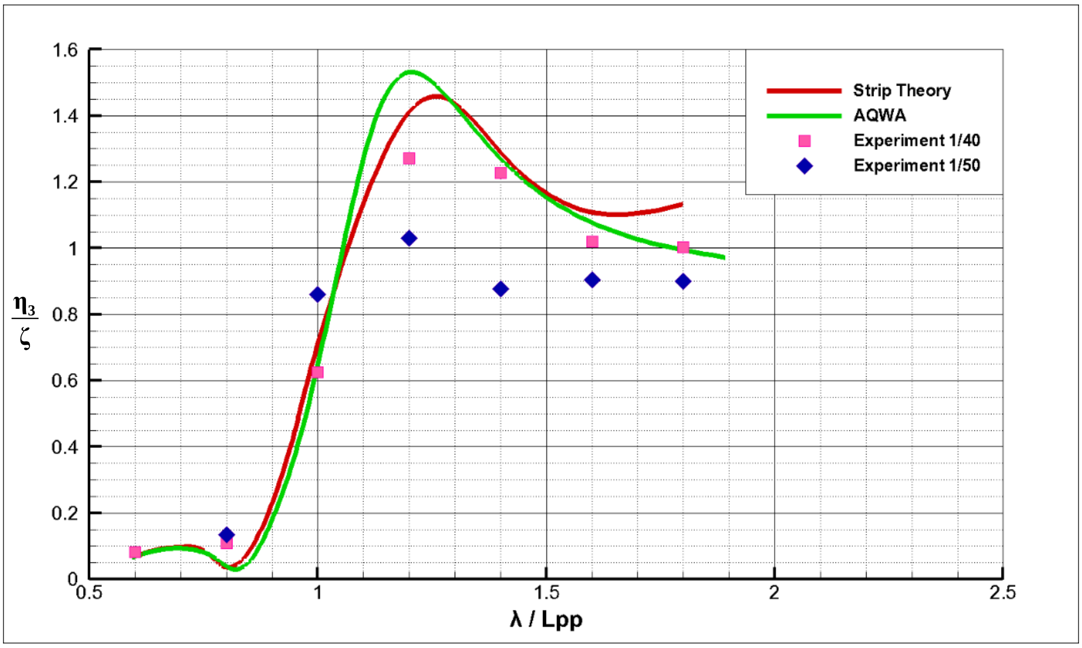

Figure 4-22 : Heave result Fn = 0.20

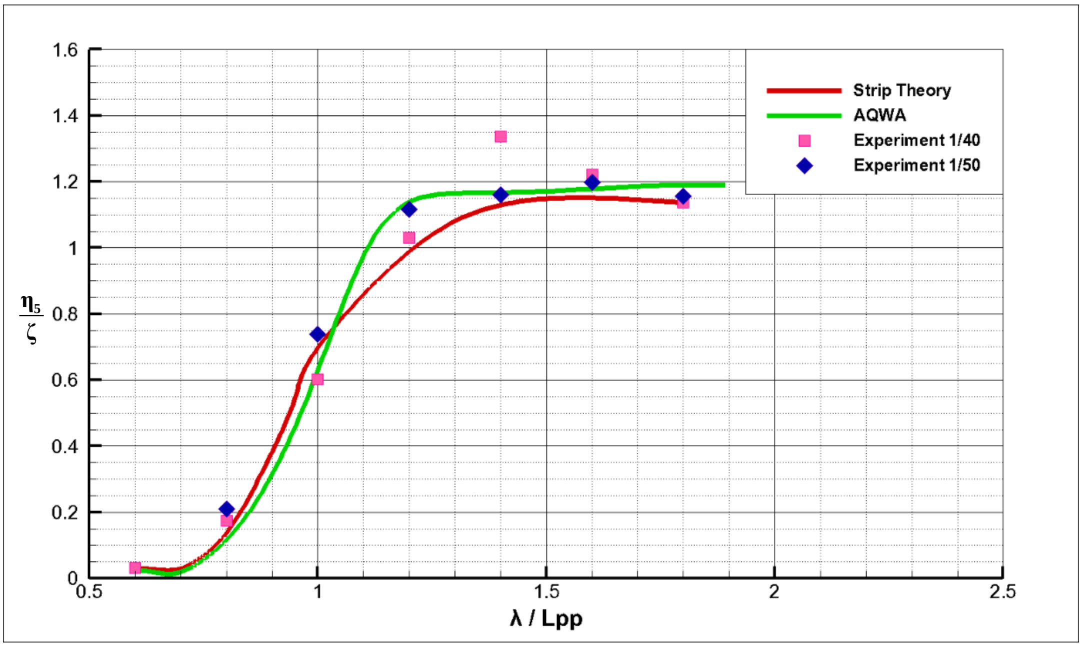

Figure 4-23 : Non-dimensional pitch result Fn = 0.20

4.4 Comparison of experimental results of 5415 type US Navy Combatant motions and accelerations with 3D panel method

In this study, the heave and pitch motions and vertical acceleration of DTMB 5415 type combatant form experimental results (INSEAN) are compared with AQWA results.

Heave and pitch are complex harmonic motions:

$$\eta_3(\omega) = \overline{\eta_3}\cos(\omega_e t + \varepsilon_3)$$

$$\eta_5(\omega) = \overline{\eta_5}\cos(\omega_e t + \varepsilon_5)$$

To obtain the non-dimensional midship acceleration from heave result, (4.2) is employed.

$$a_{\text{midship}} = \omega^2 . \overline{\eta_3} . \frac{L_{BP}}{g} \tag{4.2}$$

The principle of superposition of two simple harmonic motions is employed to obtain the bow (4.3) and stern (4.4) non-dimensional accelerations from heave and pitch results.

$$a_{\text{bow}} = \left[\left|\overline{\eta_3}\right|^2 + \left(\left|\overline{\eta_5}\right| . x_{bow}\right)^2 + 2\left|\overline{\eta_3}\right|\left|\overline{\eta_5}\right|\cos\delta \right] . \frac{L_{BP}}{g} \tag{4.3}$$

$$a_{\text{stern}} = \left[\left|\overline{\eta_3}\right|^2 + \left(\left|\overline{\eta_5}\right| . x_{stern}\right)^2 + 2\left|\overline{\eta_3}\right|\left|\overline{\eta_5}\right|\cos\delta \right] . \frac{L_{BP}}{g} \tag{4.4}$$

where $\delta = \varepsilon_5 - \varepsilon_3$.

In acceleration calculations X_{stern} = 2.5 m and X_{bow} = 3.8 m are assumed.

4.4.1 Experimental model for DTMB 5415

Main dimensions and radius of gyration for experimental model of DTMB 5415 (SIMMAN, 2014) are presented in Table 4-9.

Table 4-9 : Main dimensions and radius of gyration of DTMB 5415 for the experiment

Scale =	24.830	
L_{BP} =	5.719	m
L_{WL} =	5.726	m
B =	0.768	m
T =	0.248	m
Volumetric displacement =	0.554	m^3
C_M =	0.821	
LCG length =	-0.026	from midship (+ fwd) m
k_{XX}, 0.25*L_{BP} =	1.293	m
k_{YY}, 0.25*L_{BP} =	1.293	m

The midship acceleration is measured at the center of gravity of the model while bow acceleration is measured at 5 cm forward with respect to station 20. Also, the stern acceleration is measured at the location of 10 cm forward with respect to station 1.

4.4.2 AQWA model for DTMB 5415

Main dimensions and radius of gyration of DTMB 5415 for AQWA analysis are presented in Table 4-10.

Table 4-10 : Main dimensions and radius of gyration of DTMB 5415 for AQWA model

L_{BP} =	5.719	m
L_{WL} =	5.726	m
B =	0.768	m
T =	0.248	m
Volumetric displacement =	0.5543	m^3
C_B =	0.341	
C_M =	0.820	
C_P =	0.620	
A_W =	3.399	m^2
C_{WP} =	0.773	
LCB length =	-0.036	from midship (+ fwd) m
LCF length =	-0.278	from midship (+ fwd) m
k_{XX} ,0.34*B =	0.261	m
k_{YY}, 0.25*L_{BP} =	1.293	m
k_{ZZ}, 0.26*L_{BP} =	1.293	m

The midship acceleration is calculated at the center of gravity of the model while bow acceleration is calculated at 3.8 m forward with respect to center of gravity. Also, the stern acceleration is obtained from the location of 2.5 m forward with respect to center of gravity of the model.

The AQWA analysis model is represented with 1978 elements (Figure 4-24) of which 1198 elements are diffracted (on wetted surface).

Triangular shaped panel is employed for the best representation of DTMB 5415 form especially bulbous detail for AQWA analysis. The analyses are performed with 3.071 m/s forward speed for Fn=0.41 condition.

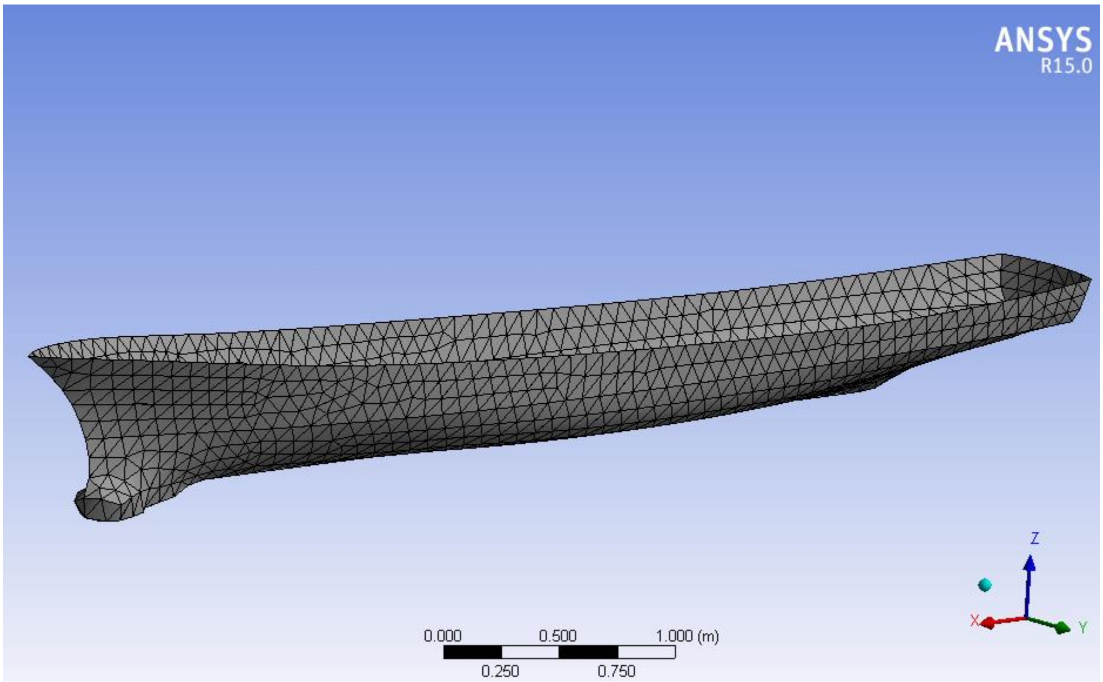

Figure 4-24 : The panel model of 5415 in AQWA

4.4.3 AQWA analysis results (Fn=0)

The results of heave and pitch analysis are presented in Table 4-11. The pitch results are non-dimensionalized by wave number, k.

Table 4-11 : AWQA heave and pitch result for Fn = 0

ω	Heave	Heave phase	Pitch	Pitch phase	1/k	$\theta_a/k\xi_a$
1.500	0.952	-0.002	0.2254	1.622	4.3600	0.9829
1.670	0.926	-0.003	0.2757	1.635	3.5175	0.9699
1.840	0.892	-0.006	0.3284	1.649	2.8976	0.9515
2.010	0.847	-0.010	0.3817	1.666	2.4282	0.9269
2.180	0.791	-0.019	0.4336	1.684	2.0642	0.8950
2.350	0.723	-0.034	0.4811	1.705	1.7764	0.8547
2.520	0.645	-0.061	0.5209	1.730	1.5448	0.8047
2.690	0.559	-0.107	0.5489	1.757	1.3557	0.7441
2.860	0.469	-0.181	0.5605	1.786	1.1993	0.6722
3.030	0.383	-0.296	0.5517	1.815	1.0685	0.5895
3.200	0.306	-0.469	0.5201	1.838	0.9580	0.4983
3.370	0.244	-0.718	0.4664	1.848	0.8638	0.4029
3.540	0.202	-1.055	0.3952	1.832	0.7828	0.3093
3.710	0.184	-1.442	0.3139	1.772	0.7127	0.2237
3.880	0.184	-1.800	0.2324	1.632	0.6516	0.1515
4.050	0.192	-2.083	0.1635	1.341	0.5981	0.0978
4.220	0.196	-2.303	0.1265	0.821	0.5509	0.0697
4.390	0.191	-2.491	0.1323	0.273	0.5090	0.0673
4.560	0.176	-2.679	0.1559	-0.056	0.4718	0.0736
4.730	0.154	-2.895	0.1709	-0.231	0.4385	0.0749
4.900	0.130	3.119	0.1668	-0.350	0.4086	0.0682

Midship, bow and stern acceleration values for AQWA analysis are presented in Table 4-12.

Table 4-12 : Midship, bow and stern vertical accelerations for Fn = 0

ω	**Midship acceleration**	**Bow acceleration**	**Stern acceleration**
1.500	1.250	1.636	1.418
1.670	1.507	2.198	1.817
1.840	1.762	2.906	2.292
2.010	1.997	3.773	2.846
2.180	2.193	4.799	3.478
2.350	2.330	5.958	4.172
2.520	2.388	7.199	4.893
2.690	2.358	8.430	5.587
2.860	2.240	9.525	6.177
3.030	2.053	10.323	6.571
3.200	1.828	10.664	6.678
3.370	1.613	10.424	6.431
3.540	1.474	9.557	5.806
3.710	1.473	8.109	4.833
3.880	1.617	6.224	3.583
4.050	1.836	4.211	2.207
4.220	2.036	2.959	1.250
4.390	2.145	3.740	1.895
4.560	2.131	5.438	3.064
4.730	2.005	6.758	3.906
4.900	1.819	7.180	4.160

The experimental values and AQWA analysis results of DTMB 5415 formed ship for Fn=0 heave and pitch motion are presented in Figure 4-25 and Figure 4-26 respectively.

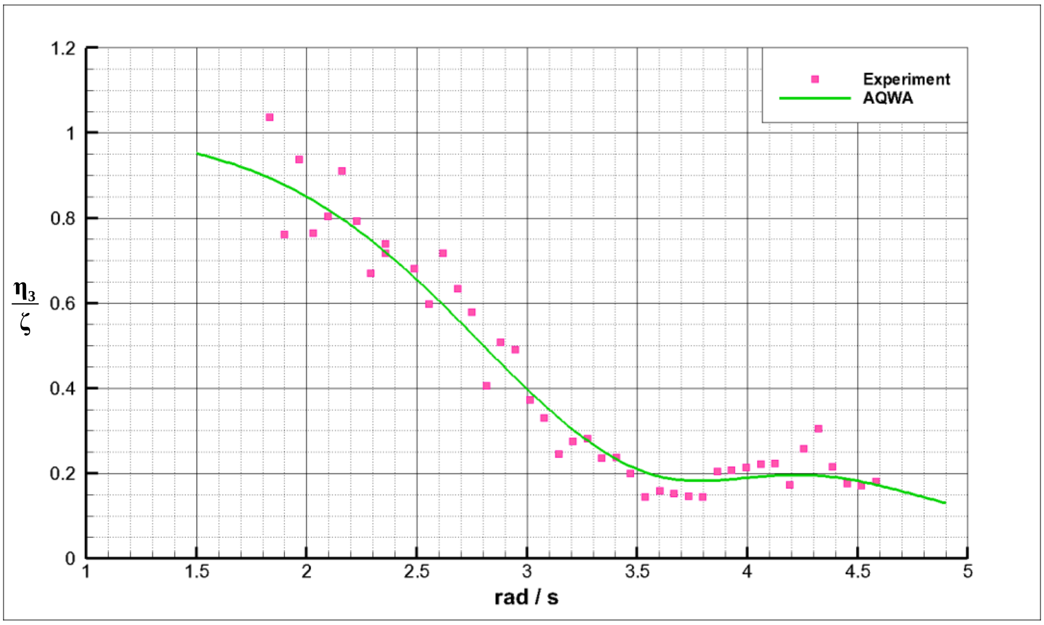

Figure 4-25 : Heave Motion Fn = 0

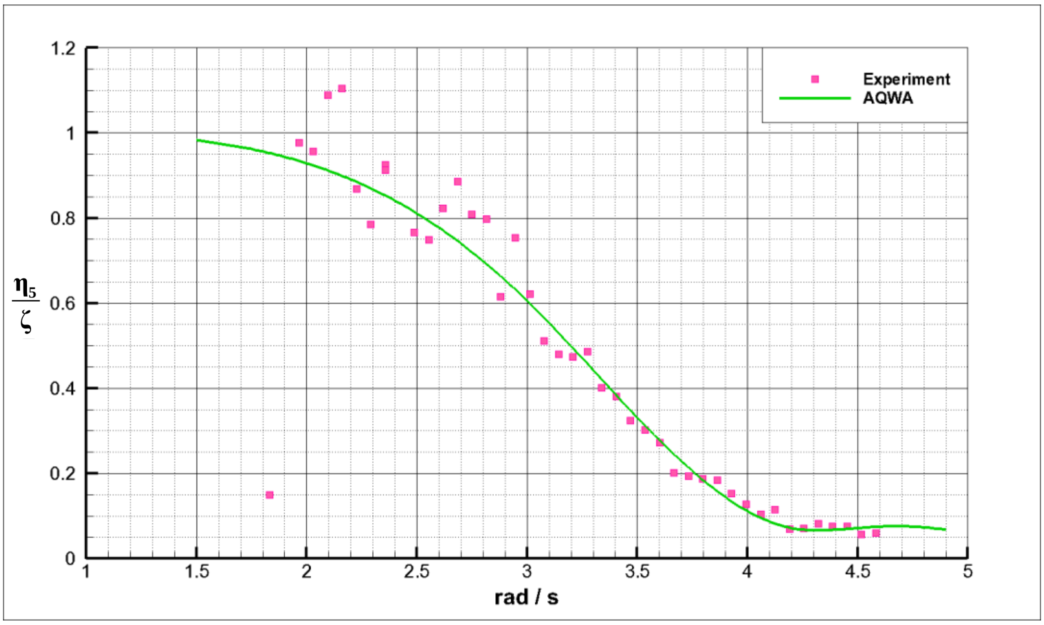

Figure 4-26 : Pitch motion Fn = 0

The experimental values and AQWA analysis results for midship, bow and stern vertical accelerations are presented in Figure 4-27, Figure 4-28 and Figure 4-29 respectively.

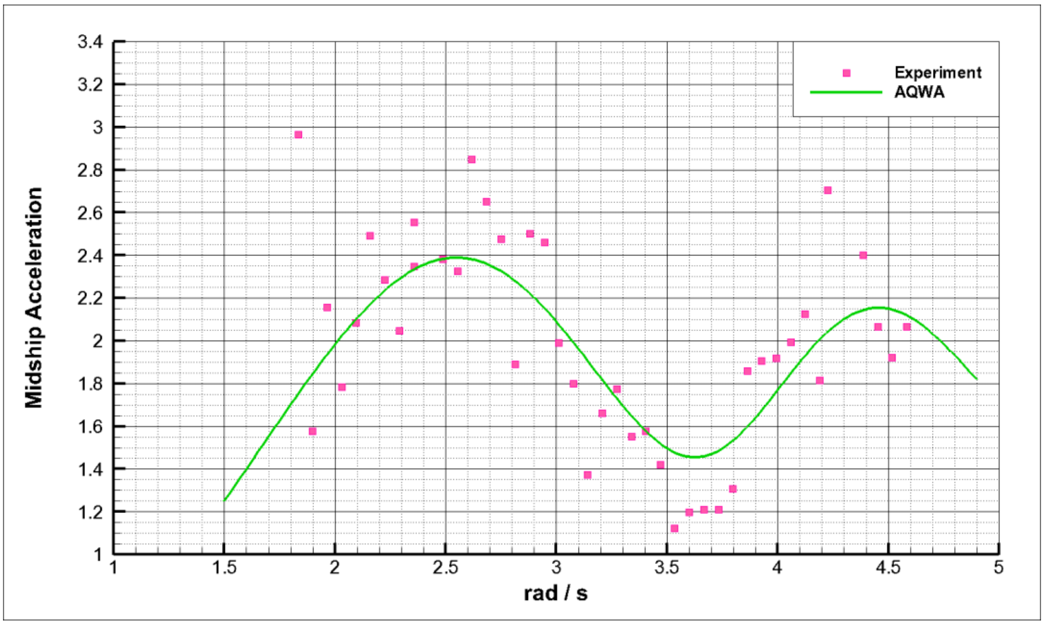

Figure 4-27 : Midship Acceleration Fn = 0

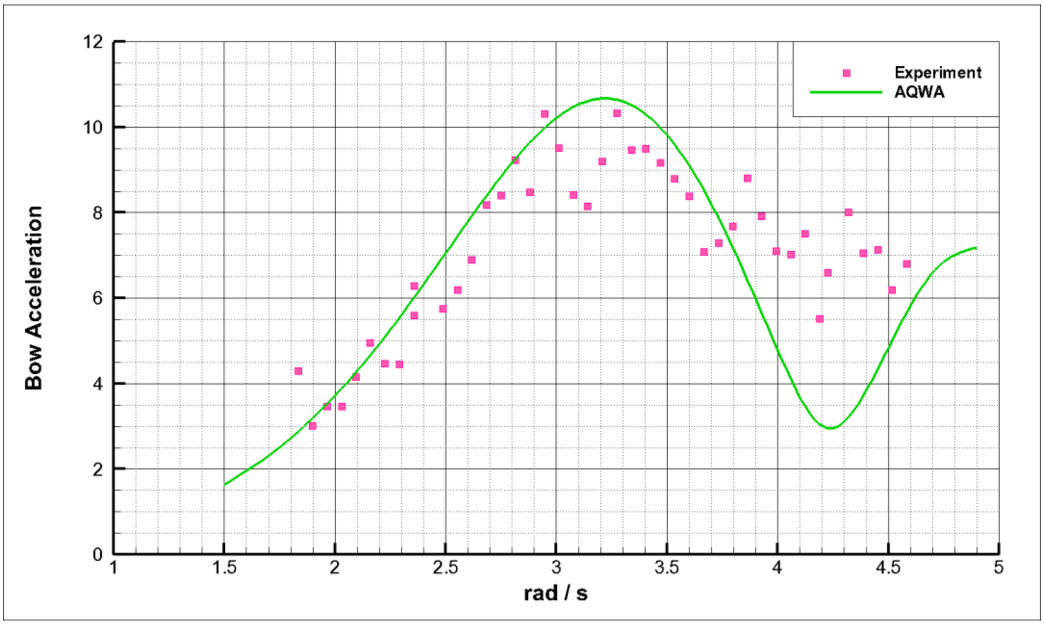

Figure 4-28 : Bow Acceleration Fn = 0

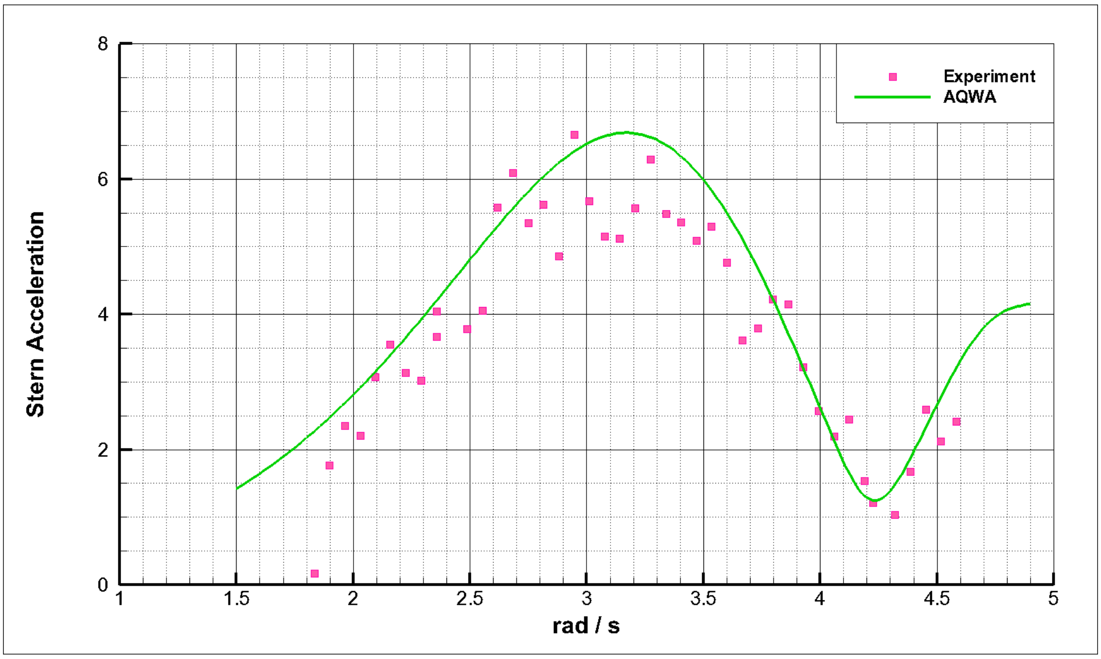

Figure 4-29 : Stern Acceleration Fn = 0

4.4.4 AQWA analysis results (Fn=0.41)

The results of heave and pitch analysis are presented in Table 4-13. The pitch results are non-dimensionalized by wave number, k.

Table 4-13 : AWQA heave and pitch result for Fn = 0.41

ω	Heave	Heave phase	Pitch	Pitch phase	1/k	$\theta_a/k\xi_a$
1.500	0.113	-0.002	0.2708	0.812	4.3600	1.1807
1.670	0.046	-0.003	0.3425	1.132	3.5175	1.2049
1.840	-0.020	-0.006	0.4139	1.399	2.8976	1.1993
2.010	-0.043	-0.010	0.4799	1.624	2.4282	1.1653
2.180	-0.024	-0.019	0.5411	1.808	2.0642	1.1169
2.350	0.022	-0.034	0.6132	1.970	1.7764	1.0893
2.520	0.118	-0.061	0.7000	2.163	1.5448	1.0814
2.690	0.318	-0.107	0.7768	2.410	1.3557	1.0531
2.860	0.662	-0.181	0.8254	2.731	1.1993	0.9900
3.030	1.167	-0.296	0.7649	-3.119	1.0685	0.8173
3.200	1.657	-0.469	0.5573	-2.701	0.9580	0.5339
3.370	1.945	-0.718	0.3479	-2.423	0.8638	0.3005
3.540	1.900	-1.055	0.2003	-2.260	0.7828	0.1568
3.710	0.399	-1.442	0.1018	-2.178	0.7127	0.0725
3.880	-0.143	-1.800	0.0383	-2.242	0.6516	0.0249
4.050	-0.203	-2.083	0.0101	2.544	0.5981	0.0060
4.220	-0.214	-2.303	0.0258	1.677	0.5509	0.0142
4.390	-0.242	-2.491	0.0332	1.619	0.5090	0.0169
4.560	-0.330	-2.679	0.0318	1.625	0.4718	0.0150
4.730	-0.589	-2.895	0.0248	1.626	0.4385	0.0109
4.900	-1.208	3.119	0.0155	1.558	0.4086	0.0063

Midship, bow and stern accelerations from the results of analysis, which is performed in AQWA, is presented in Table 4-14.

Table 4-14 : Midship, bow and stern vertical accelerations for Fn = 0.41

ω	**ω_e**	**Midship acceleration**	**Bow acceleration**	**Stern acceleration**
1.500	2.205	2.5144	5.1057	4.1710
1.670	2.543	3.2516	7.0404	5.5496
1.840	2.900	4.3622	9.4221	7.1772
2.010	3.275	5.9446	12.3504	9.1179
2.180	3.668	7.9872	16.0520	11.5207
2.350	4.079	10.6145	21.1503	14.7546
2.520	4.509	14.2431	28.0666	19.0722
2.690	4.956	18.9020	36.7334	24.6463
2.860	5.422	23.3447	47.3030	31.7435
3.030	5.905	23.3144	53.8276	36.1320
3.200	6.407	16.3291	47.5570	31.6324
3.370	6.927	8.5043	35.0549	22.9157
3.540	7.464	3.0669	23.2726	14.8940
3.710	8.020	1.4142	13.3374	8.3859
3.880	8.594	2.8345	5.4219	3.6394
4.050	9.187	3.5355	1.9367	2.4382
4.220	9.797	3.4917	5.5100	4.1643
4.390	10.425	2.9401	7.7010	5.2473
4.560	11.072	2.1219	8.1005	5.2782
4.730	11.736	1.3092	6.8761	4.3304
4.900	12.419	0.8401	4.5157	2.7141

The experimental values and AQWA analysis results of DTMB 5415 formed ship for Fn=0.41 heave and pitch motion are presented in Figure 4-30 and Figure 4-31 respectively.

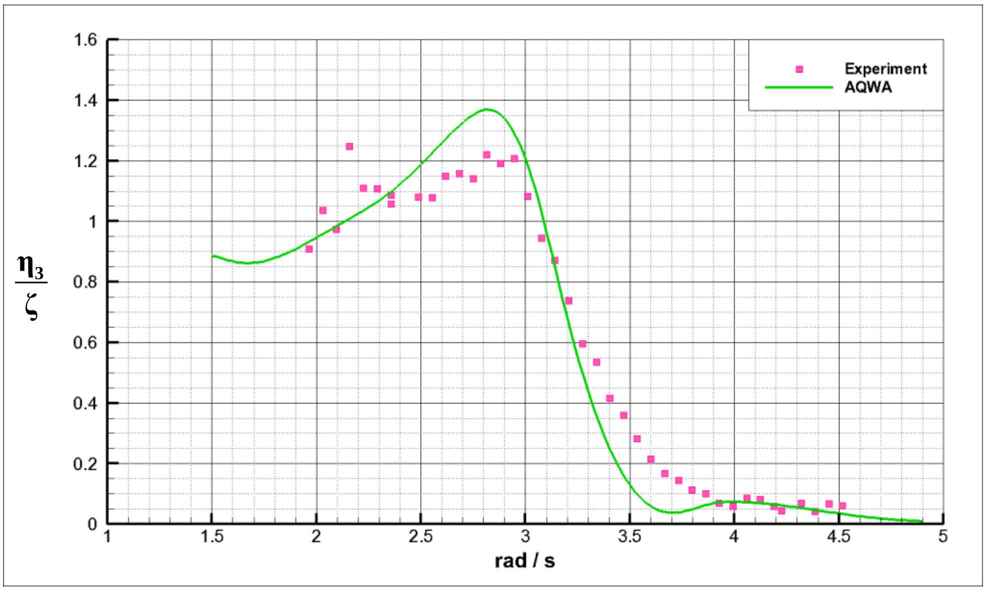

Figure 4-30 : Heave Motion Fn = 0.41

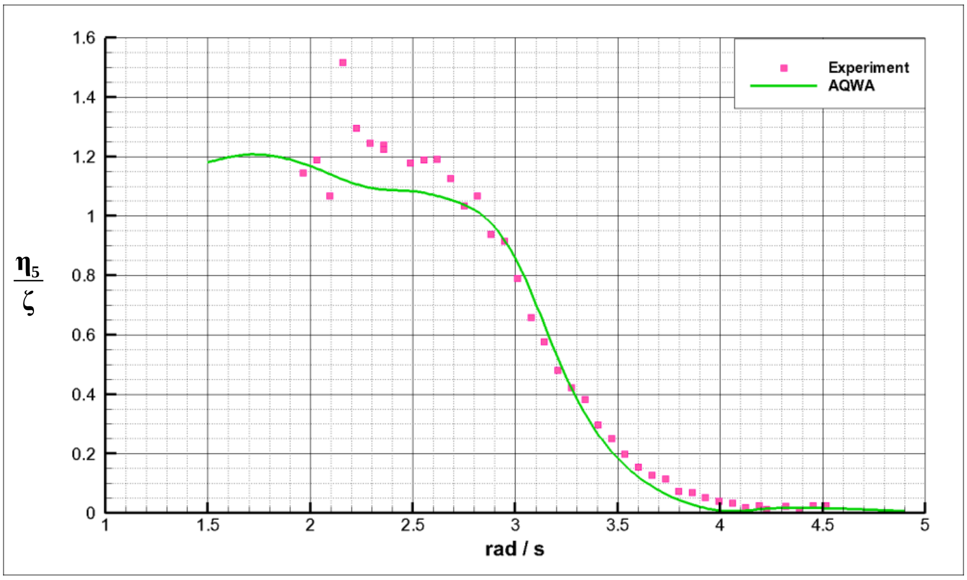

Figure 4-31 : Pitch Motion Fn = 0.41

The experimental values and AQWA analysis results for midship, bow and stern vertical accelerations are presented in Figure 4-32, Figure 4-33 and Figure 4-34 respectively.

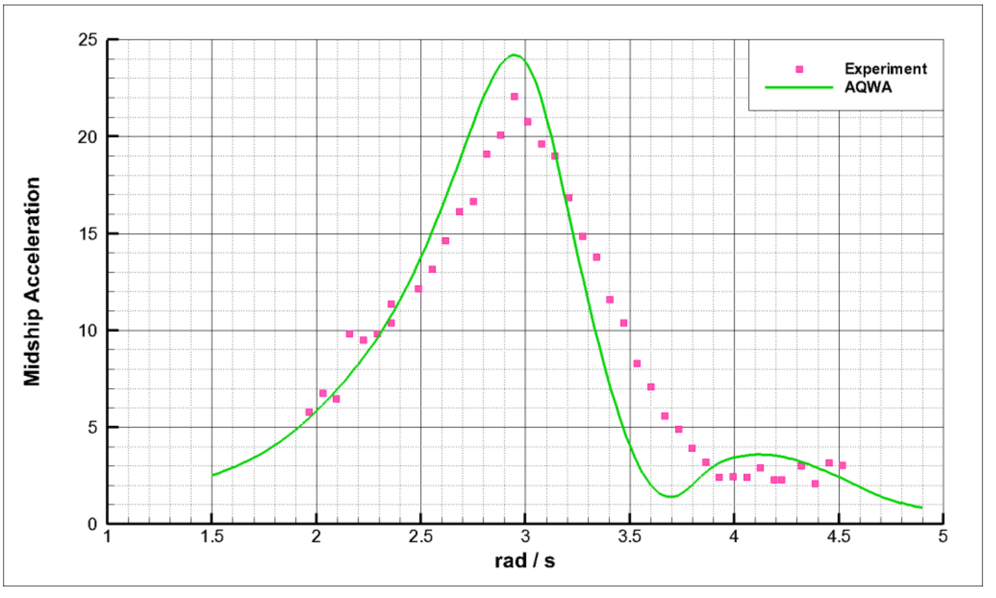

Figure 4-32 : Midship Acceleration Fn = 0.41

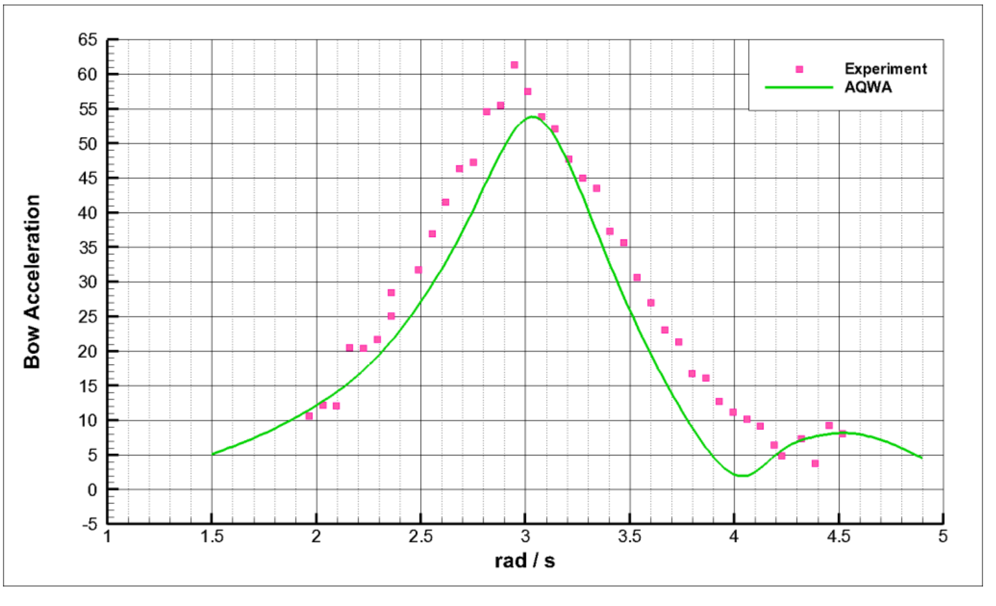

Figure 4-33 : Bow Acceleration Fn = 0.41

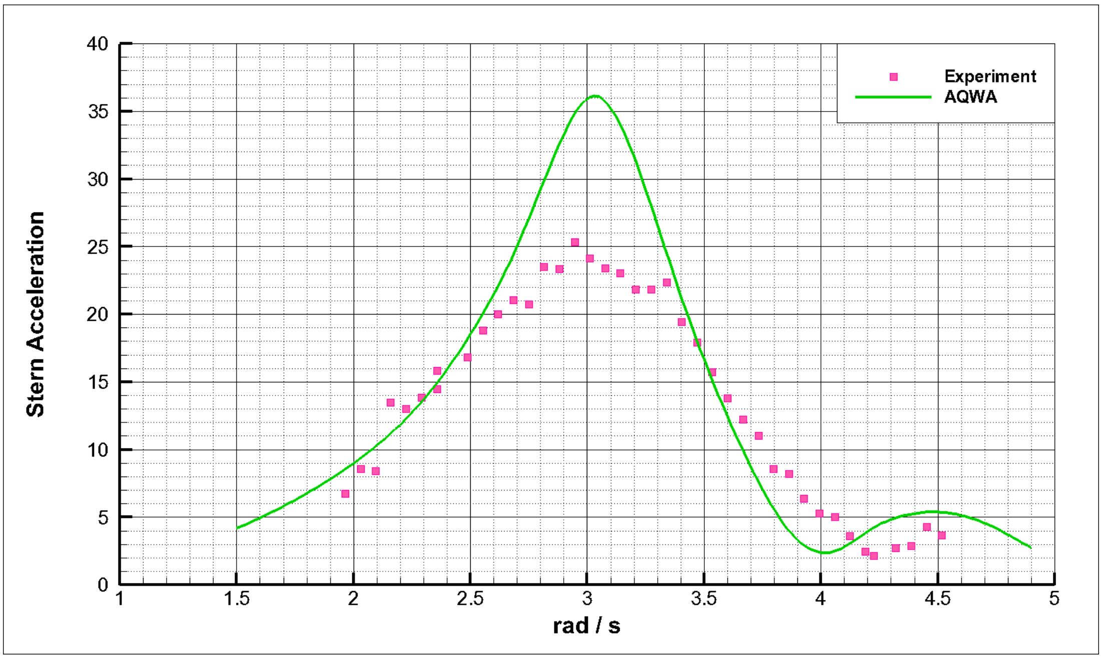

Figure 4-34 : Stern Acceleration Fn = 0.41

CONCLUSION & FUTURE WORKS

Linear seakeeping theory is one the most powerful tool to predict the seakeeping characteristics of conventional ships. It provides high accuracy and rapidly results. However, 3D panel method can be preferred for design of unconventional ship, offshore structure or prediction the motions of vessels under extreme weather conditions. Contribution of nonlinear effects due to both vessel geometry and free surface conditions is one of the important applications of 3D panel method in time domain.

In this study, the validation of experimental results and strip theory was performed for various types of floating bodies by using 3-D panel method based software ANSYS AQWA. These studies were implemented for some motions and hydrodynamic properties.

First, the validation study was carried for rectangular, cylindrical and triangular shaped floating bodies. AQWA analysis results showed good agreement with experimental values for all shapes. Some deviations were recorded in the low frequency ($\omega\sqrt{B/2g} < 0.50$) region for added mass calculation. According to the author (Vugts, 1968), these kind of discrepancies might resulted from experimental inaccuracy.

Next, a validation study was performed in order to compare the strip theory and AQWA 3-D panel method. This comparison was made for a rectangular shaped barge structure. Heave and pitch RAOs, added mass, radiation damping forces, Froude-Krylov and diffraction force components, total exciting forces and moments results are compared. Generally, all these results have shown good agreement. Froude-Krylov force values show the best agreement. Also, the results of heave & pitch motions, added mass & damping forces, diffraction forces and total exciting forces and moments of strip theory and AQWA have similar trends.

Later, the experimental values and strip theory calculation results of a Series 60 formed ship were compared with 3-D panel method. Generally, all results show good agreement for the heave and pitch motion results of Gerritsma and Beukelman (1966) both experimental and theatrical results and AQWA results, especially for the large λ/L_{BP}. However, for all results the discrepancies are initiated around $\lambda/L_{BP}=1$.

Finally, experimental heave & pitch characteristics and vertical acceleration values of DTMB 5415 type model were compared with 3-D panel method for validation purpose. Heave and pitch motions were modeled for both Fn=0 and Fn=0.41 conditions. For all conditions, results show good agreement in general. Although small deviations were recorded especially for Fn=0.41 condition, the 3-D panel method acceleration results are quite compatible. The differences can be described with the reason of the limited capability of AQWA software for forward speed, Fn<0.3 (ANSYS, 2013). Also, the assumption of the locations for X_{bow} and X_{stern} may also cause these deviations.

The present work may be extended for studying the characteristics and validations of other types of motions. The coupling effects of the motions can also be studied as future work. In addition to those, the non-linear seakeeping theory for large amplitude waves can be investigated for mooring systems including drag and drift effects.

REFERENCES

ANSYS, 2013, AQWA Theory Manual.

ANSYS, 2014, Lecture Notes: ANSYS AQWA Basics & Theory.

Beck, R.F., Reed, A.M., 2001, Modern Computational Methods for Ships in a Seaway. Presented at Twenty-Third Symposium on Naval Hydrodynamics. Val de Reuil, France. September.

Beck, R.F., Dalzell, J. F., Mandel, P., Webster, W.C., 1989, Principle of naval architecture, Vol. III.

Bertram, V., 2000, Practical Ship Hydrodynamics, p.98-148

Bruzzone, D., Grasso, A., 2007, Nonlinear time domain analysis of vertical ship motions.

Chan, Hoi Sang, 1990, A three-dimensional technique for predicting first and second-order hydrodynamic forces on a marine vehicle advancing in waves.

Fang, C.C., Wu, H.T., Tsai, J.F., 2014, A time domain technique for predicting wave load and structural response on a ship in oblique waves, TEAM 2014, İstanbul, TURKEY

Faltinsen, O. M., 1999, Sea loads on ships and offshore structures, Cambridge University Press.

Frank, W., 1967, Oscillation of Cylinders in or below the Free Surface of Deep Fluids. Technical Report 2375, Naval Ship Research and development Centre, Washington DC, USA.

Gerritsma, IR J., Beukelman, W., 1966, Comparison of calculated and measured heaving and pitching motion of a series 60, C_B= .70 ship model in regular longitudinal waves, The Seakeeping Committee of the International Towing Tank Conference, Japan

Journee, J.M.J. , Massie, W.W., 2001, Offshore Hydromechanics, Delft University of Technology.

Journée, J.M.J. , Adegeest L.J.M., 2003, Theoretical Manual of “SEAWAY for Windows”.

Journée, J.M.J., Vantorre, M., 2003, Validation of the Strip Theory Code SEAWAY by Model Tests in Very Shallow Water, Flanders hydraulics research, Numerical modelling colloquium, Antwerp, Belgium.

Holthuijsen, L.H., 2007, Waves in oceanic and coastal waters, Cambridge University Press.

Korvin-Kroukovsky, B. V., 1961, Theory of Seakeeping, The society of Naval Architects and Marine Engineers

Korvin-Kroukovsky, B. V., Jacobs, W.R., 1957, Pitching and Heaving Motions of a Ship in Regular Waves,Transactions SNAME

Lewis, F. M., 1929, The Inertia of Water Surrounding a Vibrating Ship, Transactions SNAME, Vol. 37

Okan, M. B., 2007, Gemilerin düşük hızlarda dalgalar arasındaki hareketlerinin incelenmesi için sayısal bir yöntem.

Okan, M. B., Karayel, H. B., 2008, Gemilerin dalgalar arasındaki hareketinin incelenmesi için bir yöntem, Gemi İnsaatı ve Deniz Teknolojisi Teknik Kongresi, Kasım 24-25, 2008 TMMOB Gemi Mühendisleri Odası, İstanbul.

Okan, M. B., 2010, Gemilerin dalgalar arasındaki hareketlerinin dinamik analizi için sayısal bir yöntem gelistirilmesi : teorik ve deneysel bir çalısma.

Salvesen, N., Tuck , E.O. and Faltinsen , O.M., 1970, Ship Motions and Sea Loads, SNAME, Vol. 78.

Tasai, F., 1959, On the Damping Force and Added Mass of Ships Heaving and Pitching, Technical report, Research Institute for Applied Mechanics, Kyushu University

Ursell, F., 1949, On the Heaving Motion of a Circular Cylinder on the Surface of a Fluid, Quarterly Journal of Mechanics and Applied Mathematics

Vugts, J. H., 1968, The Hydrodynamic Coefficients for Swaying, Heaving and Rolling Cylinders in a Free Surface

Url-1 < *http://www.simman2014.dk* >, date retrieved 05.10.2014.

CURRICULUM VITAE

Name Surname: Burak Tunç ÇEKİRDEKÇİ

Place and Date of Birth: Trabzon / 17.07.1985

Address: Altıntepe Mah. Değirmen Yolu Cad. No:96/18 Maltepe/İSTANBUL

E-Mail: bcekirdekci@gmail.com

B.Sc.: Shipbuilding and Ocean Engineer

Professional Experience and Rewards:

12.2011 - … **FIGES A.S. , İstanbul (Structural Analysis Engineer)**

- Performing linear and non-linear structure, thermal, linear buckling and modal analyses both commercial and military projects with ANSYS Workbench and APDL for various industries such as marine, automotive, energy etc.
- Training customers in ANSYS Workbench, ANSYS Design Modeler and ANSYS APDL.
- Providing technical support to customers for ANSYS products and carrying out benchmark studies.

02.2011 - 12.2011 **Tomay Design & Consultancy, İstanbul (Design and Structural Analysis Engineer)**

- Static structural analyses of new building and redesigned vessels and barges with ANSYS Workbench and APDL
- Stability calculations for new building and redesigned vessels and barge
- 3-D Modeling of vessels and barges with Rhinoceros